

GRANT/LEWIS 91R

IN-33772

THIRD-MOMENT CLOSURE OF TURBULENCE FOR
PREDICTIONS OF SEPARATING AND REATTACHING
SHEAR FLOWS

By

R. S. Amano
Principal Investigator

and

Pankaj Goel
Research Assistant

(NASA-CR-177055) THIRD-MOMENT CLOSURE OF
TURBULENCE FOR PREDICTIONS OF SEPARATING AND
REATTACHING SHEAR FLOWS: A STUDY OF
REYNOLDS-STRESS CLOSURE MODEL Final Report
(Wisconsin Univ.) 91 p

N87-11961

Unclas

CSCL 20D G3/34 44730

October 1986

Final Report on

"A Study of Reynolds-Stress Closure Model"

The report documents research completed during the period of January
1986 through September 1986 under NASA-Lewis Research Grant No. NAG 3-
546.

TF/86/9

SUMMARY

A numerical study of computations in backward-facing steps with flow separation and reattachment, using the Reynolds stress closure is presented.

The highlight of this study is the improvement of the Reynolds-stress model (RSM) by modifying the diffusive transport of the Reynolds stresses through the formulation, solution and subsequent incorporation of the transport equations of the third moments, $\overline{u_i u_j u_k}$, into the turbulence model. The diffusive transport of the Reynolds stresses, represented by the gradients of the third moments, attains greater significance in recirculating flows. The evaluation of the third moments by existing algebraic correlations is inadequate but the third moments evaluated by the development and solution of the complete transport equations are superior than those obtained by the algebraic correlations.

A low-Reynolds number model for the transport equations of the third moments is developed and considerable improvement in the near-wall profiles of the third moments is observed. The values of the empirical constants utilized in the development of the model are recommended.

The Reynolds-stress closure is consolidated by incorporating the equations of k and ϵ , containing the modified diffusion coefficients, and the transport equations of the third moments, $\overline{u_i u_j u_k}$, into the Reynolds stress equations. Computational results obtained by the original k - ϵ model, the original RSM and the consolidated and modified RSM are compared with experimental data. Overall improvement in the

predictions is seen by consolidation of the RSM and a marked improvement in the profiles of $\overline{u_i u_j u_k}$ is obtained around the reattachment region.

CONTENTS

	<u>Page</u>
Summary	i
Contentsiii
Nomenclature	v
CHAPTER 1 Introduction.	1
1.1 Characteristics of Backward-Facing Step Flows	1
1.2 Literature Survey	4
1.3 Objectives of the Investigation	7
CHAPTER 2 Turbulence Model with Governing Equations	9
2.1 The Reynolds Stress Model	9
2.2 k - ϵ Model and its Modification.15
2.3 Transport Equations for the Third Moments (Triple Velocity Products) of Turbulence.18
2.4 Low-Reynolds Number Model for the Third Moments23
2.5 Algebraic Equations for the Third Moments of Turbulence25
CHAPTER 3 Numerical Procedure30
3.1 Formulation and Discretization of the Transport Equations30
3.2 Differencing Scheme for the Discretized Equations32
3.3 Solution of the Equations33
3.4 Boundary Conditions34
3.5 Computing Details.36
a) Grid Selection.36
b) Convergence Criterion37
c) Model Sequencing.38

CHAPTER 4 Results and Discussion of Computations in Backward-
Facing Step Flows. 40
4.1 Introduction 40
4.2 Transport Equations for Third Moments of Turbulence with
Low-Reynolds Number Model. 41
4.3 Consolidation of RSM. 43
CHAPTER 5 Concluding Remarks. 49
References 51
Figures. 56

NOMENCLATURE

a_i	total flux coefficients
a_{ij}	anisotropy of turbulence
A	area of the boundary of the numerical control volume
$A(\Pi)$	A- function for the differencing scheme
B_1, B_2, B_3	constants used in the Reynolds Stress Model
C_1, C_2	constants used for the modeling of pressure-strain redistribution in the Reynolds-Stress Model
C_A, C_B	arbitrary constants
$C_{\epsilon 1}, C_{\epsilon 2}$	coefficients used in the source term of the dissipation equation
C_k, C_ϵ	diffusion coefficients for the turbulent kinetic energy and dissipation rate equations
C_s	diffusion coefficient for the Reynolds stresses
C_{ij}	coefficients for the boundary conditions of the Reynolds stresses
C_μ	coefficient for the determination of eddy viscosity
C_ℓ	coefficient for the determination of energy dissipation rate near the wall
C_p	coefficient used in equation (2.3.14)
$C_\gamma, C_{\gamma w}$	coefficients for the pressure-strain and the near-wall low-Reynolds number model of the transport equations of $\overline{u_i u_j u_k}$
$C_{\epsilon \gamma}$	coefficient for the dissipation rate in the transport equations of $\overline{u_i u_j u_k}$
D_{ij}	diffusion rate of Reynolds stresses
D_{ijk}	diffusion rate of $\overline{u_i u_j u_k}$
G	generation rate of turbulent kinetic energy

H	step height
k	turbulent kinetic energy
p	pressure fluctuation
P	mean pressure
P_i	cell Peclet number
P_{ij}	production rate of Reynolds stresses
P_{ijk_1}	production rate of $\overline{u_i u_j u_k}$ due to mean strain rates
P_{ijk_2}	production rate of $\overline{u_i u_j u_k}$ due to interaction of the Reynolds stresses with their gradients
Re	Reynolds number
S_ϕ	source term
S_U	linearized source term
S_P	linearized source term
t	time coordinate
u	fluctuating velocity in x-direction
U	mean velocity in x-direction
U_{IN}	inlet stream velocity
U_τ	friction velocity
v	fluctuating velocity in y-direction
V	mean velocity in y-direction
x, y	Cartesian coordinates
y_1, y_2	coordinates normal and parallel to the wall
Yo	width of the channel upstream of the step
y^+	dimensionless distance from the first node to the wall
z	net distance from the walls

GREEK SYMBOLS

$\alpha_1, \alpha_5, \alpha_7, \alpha_{12}$	coefficients for the evaluation of $\overline{u_i u_j u_k}$ by the model of Cormack et al. ¹⁶
Γ_1, Γ_2	diffusion coefficients in the x- and y-direction
δ_{ij}	Kronecker delta
ϵ	dissipation rate of turbulent kinetic energy
ϵ_{ij}	dissipation rate of Reynolds stresses
ϵ_{ijk}	dissipation rate of $\overline{u_i u_j u_k}$
κ	von Karman constant
θ_{ijk}	pressure-stress correlation for $\overline{u_i u_j u_k}$
θ_{ijkw}	near-wall low-Reynolds number effect of pressure-stress correlation for $\overline{u_i u_j u_k}$
μ	dynamic viscosity
μ_t	eddy (turbulent) viscosity
ν	kinematic viscosity
ρ	density of the fluid
σ_k	turbulent Prandtl number for k
σ_ϵ	turbulent Prandtl number for ϵ
τ	shear stress
ϕ	any dependent variable
ϕ_{ij}	pressure-strain redistribution for Reynolds stresses
ϕ_{ijw}	near-wall effects in the pressure-strain redistribution for Reynolds stresses

SUBSCRIPTS

$i, j, k, \ell,$ tensor notations

E,W,N,S values at the nodes located east, west, north, and south
of the cell P

P value at the node cell P

e,w,n,s values at the cell boundaries, lying east, west, north and
south of the cell P

w wall values

SUPERSCRIPTS

— time averaged values

CHAPTER 1

INTRODUCTION

1.1 Characteristics of Backward-Facing Step Flows

The phenomena of flow separation with the consequent wake formation, reattachment and recirculation occur in a vast array of engineering applications. Engineers use it to their advantage in augmenting the performance of equipment like combustors, heat exchangers and reactors. On the other hand, they also devote considerable effort in streamlining airfoils and similar boat-tailed bodies in order to minimize the incidence of flow separation. Very often this phenomena may be held responsible for the optimal operation of a system, which just goes to show the enormous significance of being able to correctly study and model it.

Two-dimensional backward-facing step flows have been extensively used in experimental as well as theoretical (numerical) methods to study the phenomena of flow separation, recirculation and reattachment. This class of flows possesses all the important aspects of separation, recirculation and reattachment, but at the same time, owing to their geometrical simplicity, they render themselves to easier experimentation and computation, without loss of flow complexity or susceptibility to modeling modifications.

Moreover, due to greater interest in this field, there exist relatively large sets of data on such class of flows which facilitates easier validation with modeling trends. However, some of the data like measurements of higher order moments of turbulence have not yet been explored widely.

Figure 1.1 depicts the flow field and the regimes in a typical backward-facing step. The upstream boundary layer separates at the sharp corner forming a free-shear layer. The separation line is straight and fixed at the edge of the step and there is only one separated zone. The streamlines are nearly parallel to the wall at the separation point, and significant upstream influence occurs only downstream of separation.

An ordinary boundary layer develops on the upper wall separated by an inviscid core from the viscous and separation effects on the lower wall. In case of an open top geometry, however, the inviscid core (potential flow) extends upto the top forming a free shear boundary at the surface.

The separated shear layer appears to be similar to an ordinary plane-mixing layer through the first half of the separated flow region. The dividing streamline is slightly curved and the shear layer is not influenced by the presence of the walls. The important difference between the separated shear layer and the plane-mixing layer lies in the fact that the flow on the low speed side of the shear layer is highly turbulent due to the flow reversal and recirculation, unlike the low turbulence levels encountered in plane-mixing layers.

The separated shear layer curves downward in the reattachment region and impinges on the wall. A fraction of this fluid gets deflected upstream into the recirculation region due to strong adverse pressure gradients causing the formation of a chaotic primary two-dimensional and a small three-dimensional eddy inside this region. Armaly et al.⁶ report the existence of two recirculation regions on the step-side wall (inside and outside this recirculation zone), and one on the upper wall.

The length of the recirculation region varies^{6,32,56} periodically; this is attributed to a low frequency "flapping" motion of the shear layer but in the experiment of Ruderich and Fernholz⁴⁵, however, no such flapping was observed.

The shear layer is subjected to the effects of stabilizing curvature, adverse pressure gradients and strong interaction with the wall in the reattachment region. The large eddies are confined by the wall which also results in their distortion by effectively irrotational mechanisms resulting in a spectacular decrease in the Reynolds stresses and the third moments thereby leading to the transport of turbulent kinetic energy and shear stresses toward the solid wall from the region of maximum turbulent intensity.

After impinging on the wall, the remnant fluid in the reattached shear layer continues to flow downstream developing a boundary layer on the wall resulting in the formation of the redeveloping layer.

Downstream of reattachment, the Reynolds stresses and the third moments continue to decay rapidly for a distance of several step heights. Measurements of Bradshaw and Wong⁹ and Smyth⁵¹ reveal that the outer part of the reattached shear layer still has most of the characteristics of a free shear layer as many as 50 step heights downstream of reattachment verifying the persistence of large scale eddies which are developed in the separated free-shear layer.

The process of separation and reattachment in backward-facing step flows, hence, makes them rather complex, and thus much different from boundary layer or mixing layer types of flows. Therefore, the turbulence model used for predicting this class of flows should not just be capable of accounting for all these phenomena but should also possess the sophistication of being accurate in doing so. This led to the

modification and development of the Reynolds-Stress Model (RSM) by incorporating the third moments into it as shown in the subsequent sections.

1.2 Literature Survey

Turbulence models capable of predicting complex flows like those occurring inside a backward-facing step flow have been sought by many researchers. Among the existing models of turbulence, the three most popular ones are (i) k- ϵ Model, (ii) Algebraic-Stress Model (ASM) and (iii) Reynolds-Stress Model (RSM).

These models have been used^{1,2,3,5,10,13,14,39,50,53} to predict separating and recirculating flows to an acceptable degree of satisfaction, but owing to the simplifying assumptions made in their development, these models tend to be approximations of the real physical phenomenon, predicting results which may not altogether be too realistic.

The k- ϵ Model of Jones and Launder³⁰ relies on the assumption of an isotropic turbulent viscosity in the solution of the momentum equations and the equations of k and ϵ . As pointed out by Driver and Seegmiller¹⁹, this model overestimates the isotropic turbulent viscosity in recirculating flows resulting in a higher spreading rate for the shear layer thereby yielding a premature reattachment.

A similar view is shared by Thompson and Whitelaw⁵⁵ who concluded that the instantaneous reversed flow makes a positive contribution to the turbulence shear stress and therefore the isotropic (eddy) viscosity assumption may be inappropriate in regions with flow reversals. Amano and Goel⁵ compared the results obtained by the above three models for flow into a channel with a backward-facing step and found the k- ϵ model

to consistently underpredict the levels of the Reynolds stresses. Heat transfer results for flow into a pipe with a sudden expansion³ showed that the RSM improves the prediction over the k- ϵ Model.

The ASM of Rodi⁴³ is a slight improvement over the previous model because it takes into consideration the presence of Reynolds stresses in the flow field. However, the ASM does not take into account the convective and diffusive transport of the Reynolds stresses but instead, relates it to the turbulent kinetic energy leading to algebraic equations for the Reynolds stresses. Modified version of this model containing a new dissipation rate equation wherein the production rate is made more sensitive to the streamwise curvature effects was developed by Sindir⁵⁰. The ASM, generally, as shown by Driver and Seegmiller,¹⁹ results in the inability of the model to locate the peak values of the turbulent Reynolds stresses due to an inadequate treatment of either the convection or diffusion mechanism in the kinetic energy transport equation.

The RSM comprises of individual transport equations for all the Reynolds stresses, $\overline{u_i u_j}$, thus accounting for all the processes of convection, diffusion, production and dissipation of the stresses within the flow field. The diffusive transport of the Reynolds stresses is governed by the gradient of the third moments, $\overline{u_i u_j u_k}$. In order to develop an expression for this, a transport equation for the third moments was formulated¹⁵ and through simplifying assumptions^{17,25} various terms in it were dropped out to yield algebraic expressions for the third moments, in terms of the Reynolds stresses and their spatial gradients.

As shown by Cormack et al.¹⁶, these algebraic expressions give satisfactory predictions of the third moments when compared with the experimental data for flows in channels, pipes, wall-jets and mixing

layers.^{27,36,29,58}

These algebraic expressions for the third moments seemed to work satisfactorily for a simple boundary layer type of flows. However, as pointed out by Chandrsuda and Bradshaw¹², for flow in a backward-facing step, the $\overline{u_i u_j u_k}$ profiles beyond $x/H = 12.0$ had the same shape as those in a boundary layer but their magnitudes were larger by a factor of 10 or more, for the same free shear velocity, indicating a need for some correction. They also pointed out that although streamwise decrease of third moments in the outer part of the shear layer roughly follows the decrease in the shear stress or shear stress gradient, the decrease of the third moments near the wall is far more rapid than the decrease of shear-stress or intensity gradient with streamwise distance thus throwing doubt upon the usefulness of the way of expressing in terms of a gradient diffusivity even as a pragmatic means of correlating experimental data. They argued that since turbulent transport by third moments is a very significant part of the Reynolds-stress balance in mixing layers, it should be modeled with reasonable accuracy in calculation methods implying that the algebraic relations between the third moments and the Reynolds-stresses (or their gradients) are likely to be inadequate for strongly perturbed flows and that the effects of approach to a wall imply that any calculation method, intended to deal with reattaching and separating flows, should include a fairly sophisticated model for the third moments, preferably based on the transport equations of the third moments.

Parallel with the development of theoretical models, extensive experimental observations were being made on such flows using a variety of experimental techniques like laser-doppler and pulsed-wire anemometers and hot-wire probes.^{6,12,19,22,32,45,51,52} Nevertheless,

attempts at modeling the transport equations of the third moments and solving them iteratively with the transport equations of the Reynolds stresses have not been encountered in the literature to date.

1.3 Objectives of the Investigation

The literature survey points out some of the shortcomings of the turbulence models and recommends different means for improvement, some of which are considered here.

The objective of this investigation is to attempt to overcome some of these shortcomings and deficiencies and propose an improved version of the Reynolds-Stress Model of turbulence. In order to carry out and complete this study, the general features that have been aimed at and accomplished are mentioned below. The flow geometry employed is the backward-facing step.

1. Formulation and development of transport equations for the third moments and the recommendation of different empirical constants used in the modeling process.
2. Development of a low-Reynolds number model for the transport equations of the third moments in order to account for the viscous effects near the wall.
3. Consolidation of the RSM, wherein, the two momentum equations along with the equations of k , ϵ and the Reynolds stresses, containing the third moments, and the transport equations of the third moments are solved together iteratively.

Converged values of the third moments obtained by the solution of their transport equations would be used to evaluate the diffusion rates of the Reynolds stresses in their transport equations, solution of which

would enable the evaluation of diffusion rates of k and ϵ , thereby reducing the dependence on an isotropic assumption in the model.

CHAPTER 2

TURBULENCE MODEL WITH GOVERNING EQUATIONS

2.1 The Reynolds Stress Model

In order to account for the presence of the Reynolds stresses in the turbulent momentum equation, it becomes necessary to model and evaluate these Reynolds stresses suitably.

One of the most commonly used correlation is that of Boussinesq approximation wherein

$$-\overline{\rho u_i u_j} = \mu_t \left(\frac{\partial U_i}{\partial x_j} + \frac{\partial U_j}{\partial x_i} \right) - \frac{2}{3} \delta_{ij} \rho k \quad (2.1.1)$$

where μ_t is known as the "turbulent coefficient of viscosity" or "eddy viscosity" which is analogous to the concept of laminar viscosity, μ .

Substitution of equation (2.1.1) into momentum equation yields

$$\frac{\partial U_i}{\partial t} + \frac{\partial}{\partial x_j} (U_i U_j) = -\frac{1}{\rho} \frac{\partial P}{\partial x_i} + \frac{1}{\rho} \frac{\partial}{\partial x_j} [(\mu + \mu_t) \left(\frac{\partial U_i}{\partial x_j} + \frac{\partial U_j}{\partial x_i} \right)] \quad (2.1.2)$$

Equation (2.1.2) is also known as the Boussinesq Effective Viscosity Model since $(\mu + \mu_t)$ together constitute the effective laminar and turbulent viscosities.

The eddy viscosity μ_t has been further expressed as

$$\mu_t = \frac{C_\mu \rho k^2}{\epsilon} \quad (2.1.3)$$

where C_μ is a constant (= 0.09).

Since the concept of eddy viscosity is based upon the assumption of isotropic turbulence it is commonly referred to as "isotropic turbulent viscosity".

The Reynolds stresses can also be evaluated by modeling and solving the transport equation for $\overline{u_i u_j}$ explicitly.

The transport equation for the Reynolds stresses is given as

$$\frac{\partial \overline{u_i u_j}}{\partial t} + U_k \frac{\partial \overline{u_i u_j}}{\partial x_k} = - \left(\overline{u_j u_k} \frac{\partial U_i}{\partial x_k} + \overline{u_i u_k} \frac{\partial U_j}{\partial x_k} \right) \quad (I)$$

$$- 2\nu \left(\frac{\partial \overline{u_i}}{\partial x_k} \frac{\partial \overline{u_j}}{\partial x_k} \right) - \nu \left(\frac{\partial \overline{u_k}}{\partial x_i} \frac{\partial \overline{u_j}}{\partial x_k} + \frac{\partial \overline{u_k}}{\partial x_j} \frac{\partial \overline{u_i}}{\partial x_k} \right) \quad (II)$$

$$+ \frac{p}{\rho} \left(\frac{\partial \overline{u_i}}{\partial x_i} + \frac{\partial \overline{u_i}}{\partial x_j} \right) \quad (III)$$

$$- \frac{\partial}{\partial x_k} \left[\overline{u_i u_j u_k} + \frac{\overline{u_i p}}{\rho} \delta_{jk} + \frac{\overline{u_j p}}{\rho} \delta_{ik} - \nu \left(\frac{\partial \overline{u_i u_j}}{\partial x_k} + u_j \frac{\partial \overline{u_k}}{\partial x_i} + u_i \frac{\partial \overline{u_k}}{\partial x_j} \right) \right] \quad (IV) \quad (2.1.4)$$

The left side of equation (2.1.4) represents the convective transport of the Reynolds stresses and the terms on the right represent

Term I = Production

Term II = Dissipation

Term III = Pressure-Strain Redistribution

Term IV = Diffusion

Generally the second term of the dissipation and the last two terms of the molecular transport in the diffusion term are negligible. Thus for a fluid of uniform density ρ and viscosity μ , the transport equation for the Reynolds stresses may be expressed in the form

$$\frac{Du_i u_j}{Dt} = P_{ij} - \epsilon_{ij} + \phi_{ij} + D_{ij} \quad (2.1.5)$$

where

$$P_{ij} = -\overline{(u_j u_k \frac{\partial u_i}{\partial x_k} + u_i u_k \frac{\partial u_j}{\partial x_k})}$$

$$\epsilon_{ij} = 2\nu \overline{\frac{\partial u_i}{\partial x_k} \frac{\partial u_j}{\partial x_k}}$$

$$\phi_{ij} = -\frac{p}{\rho} \overline{(\frac{\partial u_i}{\partial x_j} + \frac{\partial u_j}{\partial x_i})} \quad (2.1.6)$$

$$D_{ij} = -\frac{\partial}{\partial x_k} [\overline{u_i u_j u_k} + \frac{\overline{u_i p}}{\rho} \delta_{jk} + \frac{\overline{u_j p}}{\rho} \delta_{ik} - \nu \overline{\frac{\partial u_i u_j}{\partial x_k}}]$$

Closures for the terms in equation (2.1.6) have been proposed by different researchers as shown below.

The production term P_{ij} needs no further modeling since it consists of known and available components, essentially the Reynolds stresses and the mean strain rates.

The closure for the dissipation term ϵ_{ij} has been adopted from Rotta⁴⁴ and which is also supported by several researchers, where it is assumed that

$$\epsilon_{ij} = \frac{2}{3} \delta_{ij} \epsilon \quad (2.1.7)$$

where ϵ = dissipation rate of turbulent kinetic energy.

The pressure-strain closure ϕ_{ij} has been developed independently by Naot et al.³⁸ using a two point correlation and by Launder et al.³⁴ where a fourth order tensor is employed to simulate the pressure-strain effects.

Modified versions of the pressure-strain closure containing effects due to temperature and gravitational field and resistance to large anisotropy have been proposed by different researchers^{23,35,57}.

Preliminary studies have revealed that the closure proposed by Launder et al.³⁴ gives better agreement with the experimental data and hence their closure has been retained in this study to evaluate the pressure-strain effects.

According to Launder et al.,³⁴ the closure for the pressure-strain effect is given as

$$\begin{aligned} \phi_{ij} = & -C_1 \epsilon \left(\frac{\overline{u_i u_j}}{k} - \frac{2}{3} \delta_{ij} \right) - B_1 (P_{ij} - \frac{2}{3} \delta_{ij} G) \\ & - B_2 k \left(\frac{\partial U_i}{\partial x_j} + \frac{\partial U_j}{\partial x_i} \right) - B_3 (Q_{ij} - \frac{2}{3} \delta_{ij} G) \end{aligned} \quad (2.1.8)$$

where

$$B_1 = (C_2 + 8)/11, \quad B_2 = (30C_2 - 2)/55, \quad B_3 = (8C_2 - 2)/11$$

$$C_1 = 1.5, \quad C_2 = 0.4 \quad (2.1.9)$$

$$Q_{ij} = - \left(\overline{u_i u_k} \frac{\partial U_k}{\partial x_j} + \overline{u_j u_k} \frac{\partial U_k}{\partial x_i} \right) \quad (2.1.10)$$

$$P_{ij} = - \left(\overline{u_j u_k} \frac{\partial U_i}{\partial x_k} + \overline{u_i u_k} \frac{\partial U_j}{\partial x_k} \right) \quad (2.1.11)$$

and

$$G = - \overline{u_i u_j} \frac{\partial U_i}{\partial x_j} \quad (2.1.12)$$

In order to model and approximate the diffusive mechanism of $\overline{u_i u_j}$, the relative magnitudes of the various terms comprising the diffusive terms were investigated.

The second and third parts in the bracket of D_{ij} in equation (2.1.6) have been experimentally known to be much smaller than the third moments $\overline{(u_i u_j u_k)}$ and are consequently neglected. This is seen from the experimental data of Irvin²⁹ for self-preserving jets in an adverse pressure gradient. The profile for the total diffusion of the Reynolds stresses was nearly of the same magnitude as that obtained by the term of the third moments $\overline{(u_i u_j u_k)}$, indicating that the diffusive effects exercised by the pressure fluctuations and viscous action are negligible compared with those due to $\overline{u_i u_j u_k}$. However, we still keep the viscous term in order to account for the wall effect.

Therefore, following Daly and Harlow¹⁷, as explained in Section 2.5, the diffusive transport term is cast as

$$D_{ij} = C_s \frac{\partial}{\partial x_k} \left(\frac{k}{\epsilon} \overline{u_k u_l} \frac{\partial \overline{u_i u_j}}{\partial x_l} \right) \quad (2.1.13)$$

The turbulence model described above has been known to give satisfactory results for sudden expansions in circular pipes,³ and for plane backward facing step channels⁵.

In order to get as close to the real phenomenon as possible, the diffusive mechanism of the Reynolds stresses should be evaluated in terms of the third moments, $\overline{u_i u_j u_k}$, explicitly. This modification and

improvement is discussed in the subsequent section.

Upon comparison of results obtained by the above formulations ((2.1.5) through (2.1.13)) with the experimental data for homogeneous free shear layers and near-wall turbulence, Launder et al.³⁴ found that the near-wall streamwise stress component is appreciably larger and the transverse component much smaller than in the homogeneous free shear layer. The levels of the shear stress component \overline{uv} were also much smaller in the near-wall flow. Thus, in order to compensate for this phenomenon, Launder et al.³⁴ proposed an additional wall term, ϕ_{ijw} , to be added to equation (2.1.5). The modeling of this term is similar to the modeling of the pressure-strain term ϕ_{ij} of equations (2.1.8) such that its presence tends to increase the anisotropy of the normal stresses but tends to diminish the shear stress.

According to Launder et al.,

$$\phi_{ijw} = \left[0.125 \frac{\epsilon}{k} (\overline{u_i u_j} - \frac{2}{3} k \delta_{ij}) + 0.015 (P_{ij} - Q_{ij}) \right] \frac{k^{3/2}}{\epsilon z} \quad (2.1.14)$$

where Q_{ij} and P_{ij} are given by equations (2.1.10) and (2.1.11) respectively and z is the net distance from the walls described as

$$\frac{1}{z} = \frac{1}{x} + \frac{1}{y}$$

With the incorporation of equation (2.1.14) into equation (2.1.5), the Reynolds-Stress Equation can be written as

$$\frac{D \overline{u_i u_j}}{Dt} = P_{ij} - \epsilon_{ij} + \phi_{ij} + D_{ij} + \phi_{ijw} \quad (2.1.15)$$

2.2 k-ε Model and Its Modifications

To determine the transport equation for k , the unaveraged transport equation for a single fluctuating velocity component u_i is multiplied by u_i and then time averaged. Since $k = \overline{u_i^2}/2$, the above operation yields

$$\overline{u_i \frac{\partial u_i}{\partial t}} = \frac{\overline{\partial u_i^2/2}}{\partial t} = \frac{\partial k}{\partial t} \quad (2.2.1)$$

and the resulting equation yields as

$$\begin{aligned} \frac{\partial k}{\partial t} + U_j \frac{\partial k}{\partial x_j} = & \overline{-u_i u_j} \frac{\partial U_i}{\partial x_j} - \frac{\partial}{\partial x_j} \left(\frac{\overline{u_i^2 u_j}}{2} + \frac{\overline{p u_j}}{\rho} - \nu \frac{\partial k}{\partial x_j} \right) \\ & - \nu \left(\frac{\partial u_i}{\partial x_j} \right) \left(\frac{\partial u_i}{\partial x_j} \right) - \overline{u_i u_j} \frac{\partial u_i}{\partial x_j} \end{aligned} \quad (2.2.2)$$

The term

$$\overline{-u_i u_j} \frac{\partial U_i}{\partial x_j}$$

is the generation rate of the kinetic energy and upon invoking the Boussinesq's approximation, can be written as

$$G = \overline{-u_i u_j} \frac{\partial U_i}{\partial x_j} = \frac{\mu_t}{\rho} \left(\frac{\partial U_i}{\partial x_j} + \frac{\partial U_j}{\partial x_i} \right) \left(\frac{\partial U_i}{\partial x_j} \right) \quad (2.2.3)$$

The second term on the right side of equation (2.2.2) represents the diffusion rate and is modeled as

$$= \frac{1}{\rho} \frac{\partial}{\partial x_j} \left[\left(\mu + \frac{\mu_t}{\sigma_k} \right) \frac{\partial k}{\partial x_j} \right] \quad (2.2.4)$$

Approximating the dissipation rate ϵ by

$$- \nu \overline{\left(\frac{\partial u_i}{\partial x_j}\right)^2}$$

and neglecting other terms, the final transport equation for k reduces to

$$\frac{Dk}{Dt} = \frac{1}{\rho} \frac{\partial}{\partial x_j} \left[\left(\mu + \frac{\mu_t}{\sigma_k} \right) \frac{\partial k}{\partial x_j} \right] - \epsilon + G \quad (2.2.5)$$

where σ_k represents the turbulent Prandtl number for turbulent kinetic energy. Likewise, the transport equation for dissipation rate ϵ is obtained by differentiating the unaveraged transport equation for u_i with respect to x_l and then multiplying this equation through by $2\nu \frac{\partial u_i}{\partial x_l}$ and finally time averaging the resulting equation. The final form of this equation is,

$$\frac{D\epsilon}{Dt} = \frac{1}{\rho} \frac{\partial}{\partial x_j} \left[\left(\mu + \frac{\mu_t}{\sigma_\epsilon} \right) \frac{\partial \epsilon}{\partial x_j} \right] + C_{\epsilon 1} \frac{\epsilon}{k} G - C_{\epsilon 2} \frac{\epsilon^2}{k} \quad (2.2.6)$$

where $C_{\epsilon 1}$ and $C_{\epsilon 2}$ are constants equal to 1.44 and 1.92, respectively, and σ_ϵ is the turbulent Prandtl number for dissipation rate.

In the modeling of the turbulent diffusive transport mechanism of kinetic energy k , the third moments, ~~are~~

$$\frac{\overline{u_i^2 u_j}}{2}$$

in equation (2.2.2) are decomposed into the products of Reynolds stresses using Daly and Harlow's¹⁷ approximation of equation (2.1.13). A further assumption of isotropy led to the simplified diffusion rates as shown in equation (2.2.4).

Likewise, the turbulent diffusive transport mechanism of the dissi-

pation rate ϵ was decomposed by Hanjalic and Launder²⁵ as being proportional to

$$\frac{k}{\epsilon} \frac{\partial \epsilon}{\partial x_j} - u_i u_j \frac{\partial k}{\partial x_j}$$

and a further assumption of isotropy led to the final form of equation (2.2.6).

A low-Reynolds number model was developed by Jones and Launder^{30,31} to predict laminarization phenomenon, in which additional terms bearing functional viscosities were incorporated in the k- and ϵ -equations.

Both the high and low-Reynolds number versions of k- ϵ Model were applied by Amano and Goel² for computing the flow in a circular pipe having a sudden expansion. Computed values of the Nusselt numbers were generally close to the experimentally determined data of Amano et al.¹

A better modeling of the turbulent diffusive transport processes of k and ϵ could be attained by not resorting to the Boussinesq's eddy viscosity assumption but instead, by evaluating the diffusive transport in terms of the Reynolds stresses in their original form. Thus, the modified versions of k- and ϵ -equations can be expressed as

$$\frac{Dk}{Dt} = \frac{1}{\rho} \frac{\partial}{\partial x_j} \left[\mu \frac{\partial k}{\partial x_j} + C_k \rho \frac{k}{\epsilon} u_i u_j \frac{\partial k}{\partial x_i} \right] - \epsilon + G \quad (2.2.7)$$

$$\frac{D\epsilon}{Dt} = \frac{1}{\rho} \frac{\partial}{\partial x_j} \left[\mu \frac{\partial \epsilon}{\partial x_j} + C_\epsilon \rho \frac{k}{\epsilon} u_i u_j \frac{\partial \epsilon}{\partial x_i} \right] + C_{\epsilon 1} \frac{\epsilon}{k} G - C_{\epsilon 2} \frac{\epsilon^2}{k} \quad (2.2.8)$$

where C_k and C_ϵ are the diffusion coefficients for k and ϵ , which have been originally recommended to be equal to 0.30 and 0.15, respectively. However, upon further investigation, these coefficients have been

recommended to be 0.10 and 0.30, respectively in this study. The generation rate, G , is accordingly evaluated by using the expression given by equation (2.1.12).

2.3 Transport Equations for the Third Moments (Triple Velocity Products) of Turbulence

As discussed in Section 2.1, the turbulent diffusion of the Reynolds stresses is governed by the gradients of the third moments (equation (2.1.6)). This is expressed, employing Daly and Harlow's¹⁷ model, in terms of the product of the Reynolds stresses and their gradients (equation (2.2.13)).

In order to obtain a transport equation for $\overline{u_i u_j u_k}$, the transport equation for a single fluctuating component of velocity u_i is multiplied by $u_j u_k$ and added to the two other forms of this equation obtained by interchanging the indices i, j, k , and finally time averaging as follows

$$\frac{\overline{Du_i u_j u_k}}{Dt} = \overline{u_j u_k \frac{Du_i}{Dt}} + \overline{u_i u_k \frac{Du_j}{Dt}} + \overline{u_i u_j \frac{Du_k}{Dt}} \quad (2.3.1)$$

As shown by Chou,¹⁵ this leads to the following transport equation for $\overline{u_i u_j u_k}$

$$\frac{\overline{Du_i u_j u_k}}{Dt} = - \overline{(u_i u_j u_l \frac{\partial U_k}{\partial x_l} + u_j u_k u_l \frac{\partial U_i}{\partial x_l} + u_k u_i u_l \frac{\partial U_j}{\partial x_l})} \quad (I)$$

$$+ \overline{(u_i u_j \frac{\partial u_k u_l}{\partial x_l} + u_j u_k \frac{\partial u_i u_l}{\partial x_l} + u_k u_i \frac{\partial u_j u_l}{\partial x_l})} \quad (II)$$

$$-\overline{[u_i u_j \frac{\partial u_k u_l}{\partial x_l} + u_j u_k \frac{\partial u_i u_l}{\partial x_l} + u_k u_i \frac{\partial u_j u_l}{\partial x_l}]} \quad (III)$$

$$-\frac{1}{\rho} \overline{(u_i u_j \frac{\partial p}{\partial x_k} + u_j u_k \frac{\partial p}{\partial x_i} + u_k u_i \frac{\partial p}{\partial x_j})} \quad (IV)$$

$$\begin{aligned} & + \overline{u_i u_j \frac{\partial}{\partial x_l} [\nu (\frac{\partial u_k}{\partial x_l} + \frac{\partial u_l}{\partial x_k})]} \\ & + \overline{u_j u_k \frac{\partial}{\partial x_l} [\nu (\frac{\partial u_i}{\partial x_l} + \frac{\partial u_l}{\partial x_i})]} \\ & + \overline{u_k u_i \frac{\partial}{\partial x_l} [\nu (\frac{\partial u_j}{\partial x_l} + \frac{\partial u_l}{\partial x_j})]} \end{aligned} \quad (2.3.2)$$

(V)

Equation (2.3.2) represents the transport of the third moments, $\overline{u_i u_j u_k}$, and shows how their convective transport is balanced by other terms which represent the combined transport effects due to generation, diffusion, pressure stress and dissipation.

Terms I and II represent the production rates of $\overline{u_i u_j u_k}$ due to the action of mean strains and the shear stresses. They need no further modification being rather explicit in their form.

Term III may be rearranged as

$$\text{Term III} = - \frac{\partial}{\partial x_l} \overline{(u_i u_j u_k u_l)} \quad (2.3.3)$$

indicating its diffusive nature.

Further simplification of equation (2.3.3) is adapted from Hanjalic and Launder²⁵ in which the quadruple velocity correlations are expressed in terms of Reynolds stresses as

$$\overline{u_i u_j u_k u_l} = \overline{u_i u_j} \overline{u_k u_l} + \overline{u_i u_k} \overline{u_j u_l} + \overline{u_i u_l} \overline{u_k u_j} \quad (2.3.4)$$

Differentiating equation (2.3.4) with respect to x_l and adding it to Term II yields

$$\text{Term II} + \text{Term III} = -\left[\overline{u_i u_l} \frac{\partial \overline{u_j u_k}}{\partial x_l} + \overline{u_j u_l} \frac{\partial \overline{u_k u_i}}{\partial x_l} + \overline{u_k u_l} \frac{\partial \overline{u_i u_j}}{\partial x_l} \right] \quad (2.3.5)$$

Equation (2.3.5), hitherto, represents the production rate of $\overline{u_i u_j u_k}$ due to the interaction of Reynolds stresses with their gradients. Term IV indicates the pressure-stress effects and contains the combined effects of generation and redistribution. The modeling of the pressure-stress term is analogous to the modeling of the pressure-strain redistribution term of the Reynolds stresses in equation (2.1.8).

Term IV is evaluated by first forming the Poisson equation for fluctuating pressure p by differentiating a transport equation for u_i with respect to x_i . Upon changing the subscript j to l and the subscript i to k yields

$$\frac{1}{\rho} \frac{\partial^2 p}{\partial x_k^2} = - \frac{\partial}{\partial x_k} \left[\frac{\partial}{\partial x_l} (\overline{u_k u_l} - \overline{u_k u_l}) \right] - 2 \frac{\partial u_l}{\partial x_k} \frac{\partial U_k}{\partial x_l} \quad (2.3.6)$$

Integrating this equation with respect to x_k once and then multiplying it by $u_i u_j$ and finally time averaging the resulting equation yields

$$\frac{\overline{u_i u_j}}{\rho} \frac{\partial p}{\partial x_k} = - \overline{u_i u_j} \int \left[\frac{\partial}{\partial x_k} \left[\frac{\partial}{\partial x_l} (\overline{u_k u_l} - \overline{u_k u_l}) \right] + 2 \left[\frac{\partial u_l}{\partial x_k} \frac{\partial U_k}{\partial x_l} \right] \right] dx_k \quad (2.3.7)$$

This integral is approximated as

$$= - \overline{[u_i u_j \frac{\partial}{\partial x_\ell} (u_k u_\ell - \overline{u_k u_\ell}) + 2 \overline{u_i u_j u_\ell} \frac{\partial u_k}{\partial x_\ell}]} \quad (2.3.8)$$

Further simplification of equation (2.3.8) is done by assuming it to be equal to

$$-C_A \overline{u_i u_j u_k} \frac{\epsilon}{k} + C_B \overline{u_i u_j u_\ell} \frac{\partial u_k}{\partial x_\ell} \quad (2.3.9)$$

where C_A and C_B are arbitrary constants. Applying the approximation of equation (2.3.9) to the rest of the components in the term IV of equation (2.3.2), the final value of Term IV may be expressed as

$$\text{Term IV} = - C_\gamma \overline{u_i u_j u_k} \quad (2.3.10)$$

where the second term in equation (2.3.9) along with its coefficient is merged with Term I in equation (2.3.2) and the value of the coefficient C_γ modified accordingly to take up the deficiencies if any in making this approximation.

Term V containing the viscous effects can be rearranged and written as

$$\begin{aligned} \text{Term V} = \nu \frac{\partial}{\partial x_\ell} \overline{\left(\frac{\partial u_i u_j u_k}{\partial x_\ell} \right)} - 2\nu \left[u_i \overline{\left(\frac{\partial u_j}{\partial x_\ell} \frac{\partial u_k}{\partial x_\ell} \right)} \right. \\ \left. + u_j \overline{\left(\frac{\partial u_i}{\partial x_\ell} \frac{\partial u_k}{\partial x_\ell} \right)} + u_k \overline{\left(\frac{\partial u_i}{\partial x_\ell} \frac{\partial u_j}{\partial x_\ell} \right)} \right] \quad (2.3.11) \end{aligned}$$

The first part in equation (2.3.11) represents the viscous diffusive transport of $\overline{u_i u_j u_k}$ while the second part represents the viscous

dissipation of $\overline{u_i u_j u_k}$.

The modeling of this viscous dissipation term has been adopted from the modeling of the dissipation term ϵ_{ij} in equation (2.1.7). Owing to the similarity of the terms in equation (2.3.11) and the dissipation term (Term II in equation (2.1.4)) the dissipative effects influencing the transport of $\overline{u_i u_j u_k}$ can be expressed as

$$\text{Dissipation} = C_{\epsilon\gamma} \frac{2}{3} (\delta_{ij} + \delta_{jk} + \delta_{ik}) \epsilon k^{1/2} \quad (2.3.12)$$

where the single fluctuating velocities are set proportional to $k^{1/2}$ with the constant $C_{\epsilon\gamma}$ thrown in to account for the discrepancies, if any, in making this correlation.

Based upon parametric tests, the value of $C_{\epsilon\gamma}$ is recommended to be 0.10. Equation (2.3.2) may then finally be cast in accordance with the Reynolds-stress equation (equation (2.1.5)) as

$$\frac{D\overline{u_i u_j u_k}}{Dt} = P_{ijk_1} + P_{ijk_2} + \theta_{ijk} - \epsilon_{ijk} + D_{ijk} \quad (2.3.13)$$

where

P_{ijk_1} = production due to mean strains

$$= - C_p \left(\overline{u_i u_j u_l} \frac{\partial U_k}{\partial x_l} + \overline{u_j u_k u_l} \frac{\partial U_i}{\partial x_l} + \overline{u_k u_i u_l} \frac{\partial U_j}{\partial x_l} \right)$$

P_{ijk_2} = Production due to Reynolds stresses interacting with their gradients

$$= - \left(\overline{u_k u_l} \frac{\partial \overline{u_i u_j}}{\partial x_l} + \overline{u_j u_l} \frac{\partial \overline{u_i u_k}}{\partial x_l} + \overline{u_i u_l} \frac{\partial \overline{u_j u_k}}{\partial x_l} \right)$$

θ_{ijk} = Pressure-Stress effects

$$= - C_p \frac{\epsilon}{k} \overline{u_i u_j u_k}$$

ϵ_{ijk} = Dissipation due to viscous action

$$= C_p \frac{2}{3} (\delta_{ij} + \delta_{jk} + \delta_{ki}) \epsilon k^{1/2} \quad (2.3.14)$$

where C_p in P_{ijk} , is used to add the second term in equation (2.3.9). Solution of the transport equations of the third moments (equation (2.3.13)) would yield the values of $\overline{u_i u_j u_k}$ which when plugged into equation (2.1.5) would give the diffusion rate of the Reynolds stresses enabling a better approximation and modeling of the Reynolds-stress closure.

2.4 Low-Reynolds Number Model for the Third Moments

In order to incorporate the viscous effects that are predominant near the wall, a low-Reynolds number modification has been developed here to improve the agreement with experimental data.

The transport equation for $\overline{u_i u_j u_k}$ incorporating this low-Reynolds number model is

$$\frac{D \overline{u_i u_j u_k}}{Dt} = P_{ijk1} + P_{ijk2} + \theta_{ijk} + \theta_{ijkw} - \epsilon_{ijk} + D_{ijk} \quad (2.4.1)$$

This equation is identical to equation (2.3.13) except for the term θ_{ijkw} which is the additional pressure-stress contribution needed to distribute and control the levels of $\overline{u_i u_j u_k}$ in the viscosity dominated near-wall region.

The theory of this low-Reynolds number model is based upon the existence of three regions: i) viscous sublayer, ii) buffer layer, and iii) the fully turbulent core. The viscous sublayer exists upto a distance $y^+ \leq 10.0$ where

$$y^+ = \frac{\rho (\tau_w/\rho)^{1/2} y}{\mu}$$

In this region the dissipation rate is governed by the equation

$$\text{dissipation} = 2\nu \left(\frac{\partial k^{1/2}}{\partial y} \right)^2 \quad (2.4.2)$$

The dissipation rate in the buffer layer is formulated as

$$\text{dissipation} = C_{\gamma w} \frac{k^{3/2}}{C_\ell y} \quad (2.4.3)$$

Thus, the terms $\theta_{ijk} + \theta_{ijkw}$ are together given as

$$\theta_{ijk} + \theta_{ijkw} = C_\gamma \frac{\overline{u_i u_j u_k}}{k} \left(\epsilon + \left[\left| C_{\gamma w} \frac{k^{3/2}}{C_\ell y}, 2\nu \left(\frac{\partial k^{1/2}}{\partial y} \right)^2 \right| \right] \right) \quad (2.4.4)$$

where C_γ and $C_{\gamma w}$ are modified coefficients for the pressure-stress and its corresponding near-wall approximation. The symbol $| A, B |$ represents the largest of the arguments in this bracket.

The development and incorporation of equations (2.4.2) and (2.4.3) is based upon the near-wall model of Amano et al.,¹ where boundary conditions of the wall have been derived using these profiles for the dissipation rate.

In equation (2.4.3), C_ℓ is another constant defined as

$$C_\ell = \kappa C_\mu^{-3/4} \quad (2.4.5)$$

where κ is the von Karman constant and is equal to 0.42.

Figure 2.1 shows the variation of the dissipation rates obtained by equations (2.4.2) and (2.4.3), with the non-dimensional distance y^+ from the wall. The dissipation rate, ϵ , obtained by the solution of the ϵ -equation (equation(2.2.6)) is also shown for comparison.

As shown in the figure, the dissipation rate is considerably augmented in the near-wall region and therefore justifies the inclusion of equations (2.4.2) and (2.4.3) for correcting the near-wall values of $\overline{u_i u_j u_k}$ in the low-Reynolds number model.

The dissipation rate given by equation (2.4.2) is higher in the near-wall region but decays very rapidly with increasing distance from the wall, as seen in the figure. Thus, the incorporation of equation (2.4.4) in the transport equations of the third moments enables the viscosity dominated near-wall region to exercise its influence on the behavior of the third moments appropriately.

2.5 Algebraic Equations for the Third Moments of Turbulence

Algebraic correlations have been developed by different researchers to evaluate the third moments, without solving the complete transport equation for $\overline{u_i u_j u_k}$.

In order to arrive at these algebraic equations considerable simplifying assumptions have been made which tend to introduce imperfections in the modeling.

Based upon their experimental measurements of asymmetric flow in a plane channel, Hanjalic and Launder²⁵ found that the term P_{ijk_1} in equation (2.3.13) was negligible compared to other terms in the equation, especially for wall boundary layers. Furthermore, upon neglecting the convective transport as well as the viscous dissipation and molecular diffusion, the equation (2.3.13) reduces to

$$\theta_{ijk} = - P_{ijk_2} \quad (2.5.1)$$

Upon substituting the values of θ_{ijk} and P_{ijk_2} from equation (2.3.14) into equation (2.5.1), Hanjalic and Launder²⁵ obtained the following equation

$$\overline{u_i u_j u_k} = - 0.11 \frac{k}{\epsilon} \left[\overline{u_\ell u_j} \frac{\partial \overline{u_i u_k}}{\partial x_\ell} + \overline{u_\ell u_i} \frac{\partial \overline{u_j u_k}}{\partial x_\ell} + \overline{u_\ell u_k} \frac{\partial \overline{u_i u_j}}{\partial x_\ell} \right] \quad (2.5.2)$$

Daly and Harlow¹⁷ simplified equation (2.5.2) by suitable contraction and obtained the following correlation

$$\overline{u_i u_j u_k} = - 0.25 \frac{k}{\epsilon} \overline{u_k u_\ell} \frac{\partial \overline{u_i u_j}}{\partial x_\ell} \quad (2.5.3)$$

After further simplification, Shir⁴⁸ proposed

$$\overline{u_i u_j u_k} = - 0.04 \frac{k^2}{\epsilon} \frac{\partial \overline{u_i u_j}}{\partial x_k} \quad (2.5.4)$$

Cormack et al.¹⁶ obtained these algebraic expressions by approximating the experimentally determined profiles for $\overline{u_i u_j}$, ϵ and $\overline{u_i u_j u_k}$ with polynomials with coefficients, chosen to give a least squares fit to the data and discretized the cross-stream coordinate in each flow into a certain number of grid intervals. They used the most general model for the triple velocity correlation tensor as generated using the asymptotic approach of Lumley and Khajeh Nouri.³⁷

They obtained a set of algebraic equations and used the least squares approach to solve these set of equations and optimized the parameters. The model they obtained is as follows

$$\begin{aligned}
\overline{u_i u_j u_k} &= \left[4 \frac{k^2}{\epsilon} (2\alpha_1 (\delta_{ij} \delta_{kl} + \delta_{ik} \delta_{jl} + \delta_{kj} \delta_{il})) \frac{\partial k}{\partial x_l} \right. \\
&+ \alpha_5 (a_{ik,j} + a_{ij,k} + a_{kj,i}) \\
&+ 2 \frac{k}{\epsilon} (2\alpha_7 (\delta_{ik} a_{jl} + \delta_{ij} a_{kl} + \delta_{jk} a_{il})) \frac{\partial k}{\partial x_l} \\
&\left. + \alpha_{12} (a_{ik} a_{jl,l} + a_{ij} a_{kl,l} + a_{jk} a_{il,l}) \right] \quad (2.5.5)
\end{aligned}$$

where

$$a_{ij} = \overline{u_i u_j} - \frac{2}{3} \delta_{ij} k \quad (2.5.6)$$

and

$$a_{ij,k} = \frac{\partial a_{ij}}{\partial x_k}$$

Out of the 20 parameters (α_i) that they had started out with, they were able to determine the most significant ones as α_1 , α_5 , α_7 , and α_{12} . The values of these parameters have been recommended for various kinds of flows along with the universal values applicable to all flows wherein

$$\begin{aligned}
\alpha_1 &= -8.14 \times 10^{-3} \\
\alpha_5 &= -1.72 \times 10^{-2} \\
\alpha_7 &= -4.80 \times 10^{-2} \\
\alpha_{12} &= -1.02 \times 10^{-1} \quad (2.5.7)
\end{aligned}$$

In arriving at the above mentioned algebraic correlations (equations (2.5.2) - (2.5.5)) various simplifying assumptions had been made which necessitated the deletion of different terms from equation (2.3.13)

thus increasing the deviation from the actual physical phenomenon. A more realistic modeling would be obtained if the complete transport equation of the third moments could be solved iteratively.

Table 2.1 lists the recommended values for constants used in the present study.

Table 2.1 Recommended Values for the Constants Used in Turbulence Modeling.

B_1	$= (C_2 + 8)/11$
B_2	$= (30C_2 - 2)/55$
B_3	$= (8C_2 - 2)/11$
C_1	$= 1.5$
C_2	$= 0.4$
C_k	$= 0.10$
C_l	$= 2.548$
C_p	$= 1.0$
C_s	$= 0.25$
C_ϵ	$= 0.30$
$C_{\epsilon 1}$	$= 1.44$
$C_{\epsilon 2}$	$= 1.92$
$C_{\epsilon \gamma}$	$= 0.10$
C_μ	$= 0.09$
C_γ	$= 3.0$
$C_{\gamma w}$	$= 8.0$
κ	$= 0.42$
σ_k	$= 1.0$
σ_ϵ	$= \frac{\kappa^2 C_\mu^{-1/2}}{(C_{\epsilon 2} - C_{\epsilon 1})}$

CHAPTER 3

NUMERICAL PROCEDURE

3.1 Formulation and Discretization of the Transport Equations

The steady state 2-dimensional equations for all the parameters solved in this study can be, in general, cast and expressed as

$$\frac{\partial \rho U \phi}{\partial x} + \frac{\partial \rho V \phi}{\partial y} - \left[\frac{\partial}{\partial x} \left(\Gamma_1 \frac{\partial \phi}{\partial x} \right) + \frac{\partial}{\partial y} \left(\Gamma_2 \frac{\partial \phi}{\partial y} \right) \right] + S_\phi = 0 \quad (3.1.1)$$

where ϕ stands for different dependent variables U , V , k , ϵ , $\overline{u_i u_j}$ and $\overline{u_i u_j u_k}$. Γ_1 and Γ_2 are the corresponding diffusion coefficients in the streamwise and the normal directions to the flow respectively. The remaining terms are lumped into the source (or sink) term S_ϕ .

Equation (3.1.1) shows how the convective transport (net rate of inflow of ϕ to the cell by convective fluxes) is balanced by the diffusive transport (net rate of inflow of ϕ to cell by diffusive fluxes) and the generation or dissipation rate of ϕ within the cell. Discretization of equation (3.1.1) is carried out by dividing the computational domain into elemental control volumes and then integrating the equation over each of these control volumes. Figure 3.1 shows a typical node P inside its control volume bordered by neighboring nodes E , W , N , S (representing the east, west, north and south locations).

Following Patankar,⁴⁰ equation (3.1.1) is integrated over this control volume and thus can be written as

$$a_P \phi_P = a_E \phi_E + a_W \phi_W + a_N \phi_N + a_S \phi_S + S_U \quad (3.1.2)$$

where,

$$\begin{aligned} a_E &= D_e A(|P_e|) + [|-F_e, 0|] \\ a_W &= D_w A(|P_w|) + [|F_w, 0|] \end{aligned} \quad (3.1.3)$$

$$\begin{aligned} a_N &= D_n A(|P_n|) + [|-F_n, 0|] \\ a_S &= D_s A(|P_s|) + [|F_s, 0|] \\ a_P &= a_E + a_W + a_N + a_S - S_P \end{aligned} \quad (3.1.4)$$

and

$$\int S_\phi dVol = S_U + S_P \phi_P$$

In equation (3.1.3) $A(|P_i|)$ is a function of the cell Peclet number P_i whose formulation depends upon the type of differencing scheme being employed. The aspect of differencing scheme is discussed in the following section. The symbol $[|A, B|]$ is the same as the one used in (2.4.4).

Equation (3.1.2) is the discretized algebraic form of the original differential equation (3.1.1).

Figure 3.2 shows the staggered grid system employed in this study. The scalar cell denoted by the node P is used to discretize and compute the scalar parameters like P , k , ϵ , $\overline{u^2}$, and $\overline{v^2}$ and $\overline{u_i u_j u_k}$.

The U-momentum cell is staggered with respect to the scalar cell by shifting it by half a cell to the left while the V-momentum cell is staggered by shifting it half a cell below the scalar cell. The cell for \overline{uv} , however, is staggered by shifting it half a cell to the left and half a cell below the scalar cell as shown in the figure.

The reason for doing this staggering of the cells is the advantage gained by making the velocities available at locations where they would facilitate gradient calculation thus making it easier to satisfy the continuity equation. Likewise, the stresses are evaluated at locations

where they would enable their gradients and production rates to be evaluated easily.

3.2 Differencing Scheme for the Discretized Equations

After having transformed the original differential transport equation (equation (3.1.1)) into an algebraic equation (equation (3.1.2)), it is required to prescribe a formulation for the combination of the convective and diffusive fluxes such that the coefficients in equation (3.1.2) may be evaluated. Formulation of a scheme to combine the convective and diffusive fluxes is referred to as differencing scheme.

The differencing scheme employed in this study has been adopted from Amano et al.¹ in which the exponential (exact) scheme in Table 3.1 is expanded upto the fourth order term as

$$A(|P_i|) = [|0, (1 - \frac{1}{2} |P_i| + \frac{1}{12} |P_i|^2 - \frac{1}{720} |P_i|^4) |] \quad (3.2.1)$$

As shown by Amano et al.,¹ the deviation of the hybrid scheme from the exact exponential scheme is quite large at $P_i = \pm 2$ and so it is

TABLE 3.1. Function $A(|P_i|)$ for Different Differencing Schemes

Scheme	Function $A(P_i)$
Central differencing	$1.0 - 0.5 P_i $
Upwind	1.0
Hybrid	$[0, (1 - 0.5 P_i)]$
Exponential (Exact)	$ P / (e^{ P_i } - 1)$
Fourth Order	$[0, (1 - \frac{1}{2} P_i + \frac{1}{12} P_i ^2 - \frac{1}{720} P_i ^4)]$

rather premature to neglect the diffusion effects as soon as $|P_i|$ exceeds 2.

The fourth order scheme of equation (3.2.1) reduces to the upwind scheme and neglects the diffusion effects after $|P_i|$ becomes greater than 4 which makes it approach closer to the exponential (exact) solution. Moreover, the fourth order scheme is less expensive to compute compared to the exponential scheme, although it may involve extra expenses compared to computation with the hybrid scheme. An additional advantage of the fourth order scheme lies in the fact that unlike the hybrid scheme, it introduces very little or no false diffusion effects into the solution. False diffusion is an inherent aspect of the hybrid differencing scheme making it less accurate at high Reynolds number flows, convection dominated flows and more so, for recirculating flows.

3.3 Solution of the Equations

After having formulated and discretized the equation as shown in the previous sections, they are solved iteratively using line-by-line solution method. The initially guessed values of the flow field for various parameters is prescribed and these are improved upon from one line to the other in successive iterations.

As shown in Roache,⁴² for the solution of the equations along the nodes on each line (e.g. North-South line), values of the parameters on the neighboring lines are assumed to be temporarily known (previously stored values). The equation for each node on this North-South line then reduces to one where only three values (ϕ_P , ϕ_N and ϕ_S) are unknown. The set of equations for all nodes on the North-South line then takes a simple form in which the non-zero coefficient matrix is tri-diagonal and

which is solved by the line-by-line iterative technique called TDMA (Tri-Diagonal Matrix Algorithm).

3.4 Boundary Conditions

The numerical solution of the transport equations requires the provision of correct boundary values in the flow domain.

For backward-facing step flows, boundary conditions need to be prescribed at the walls and along the outflow section at the exit.

At the wall boundaries, the "wall law" is used to specify mean velocities, turbulence kinetic energy, the dissipation rate, the Reynolds stresses and the third moments.

For the mean velocities, the wall shear stress is determined using the velocity gradient at the wall, which is then used to prescribe the boundary values.

For the turbulent kinetic energy, the generation rate at the wall is modified by incorporating the wall shear stress in the generation rate, which is then substituted in the transport equation of k thereby introducing the effect of the wall.

The dissipation rate, however, is expressed in terms of the kinetic energy as

$$\epsilon = \frac{k^{3/2}}{C_\mu y} \quad (3.4.1)$$

which is similar to the equation (2.4.3). This value constitutes the boundary value for the dissipation rate.

For prescribing the wall values for the Reynolds stresses, Launder et al.³⁴ had obtained proportionality correlations between $\overline{u_i u_j}$ and U_τ for channel flows as

$$\overline{u_i u_j} = C_{ij} U_\tau^2 - (1 - \delta_{ij}) \frac{y_1}{\rho} \frac{dP}{dy_2} \quad (3.4.2)$$

where U_τ is the friction velocity and where y_1 and y_2 represent the coordinates normal and parallel, to the wall in consideration, respectively. The coefficients C_{ij} are given as

$$\begin{aligned} C_{11} &= 5.1 \\ C_{12} &= -1.0 \\ C_{22} &= 1.0 \end{aligned} \quad (3.4.3)$$

Using the correlation between k and U_τ in the wall proximity region, derived by Hanjalic and Launder,²⁵ as

$$k \approx 3.5 U_\tau^2 \quad (3.4.4)$$

the boundary values of equation (3.4.2) may be expressed as

$$\overline{u_i u_j} = C_{ij} k - (1 - \delta_{ij}) \frac{y_1}{\rho} \frac{dP}{dy_2} \quad (3.4.5)$$

where the coefficients C_{ij} are accordingly changed as

$$\begin{aligned} C_{11} &= 1.214 \\ C_{12} &= -0.238 \\ C_{22} &= 0.238 \end{aligned} \quad (3.4.6)$$

For prescribing the wall values for the third moments, the algebraic correlation of Shir,⁴⁸ equation (2.5.4), combined with the wall values of $\overline{u_i u_j}$, equation (3.4.5), is used as

$$\overline{u_i u_j u_k} = 0.04 \frac{k^2}{\epsilon} \frac{\partial}{\partial x_k} \left(C_{ij} k - (1 - \delta_{ij}) \frac{y_1}{\rho} \frac{dP}{dy_2} \right) \quad (3.4.7)$$

It was seen that the solution of the equation for the third moments did not seem to be affected by the choice of boundary conditions; for ins-

tance, even a value of zero at the wall did not change the solution appreciably.

For prescribing the boundary values along the outflow section, at the exit, a condition of continuous flow with zero streamwise gradients was imposed for all the parameters.

3.5 Computing Details

a) Grid Selection

In order to have a fine mesh in the recirculation and near-wall regions of the computational domain, a variable grid system was employed wherein the grid spacing increased monotonically in the downstream flow direction thus generating a fine spacing near the step and a relatively coarser mesh towards the far downstream end. In the transverse direction, however, the grid spacing was made finer near the bottom wall and it became coarser with increasing distance from this wall.

Exploratory tests were made using mesh sizes of 32 x 32, 42 x 42 and 52 x 52 with different grid expansion factors in the streamwise and transverse direction and with different axial lengths of the solution domain. Amano and Goel⁵ and Sindir⁵⁰ employed the change in reattachment length as a basis for determining the grid independency stage and thus came up with a 42 x 42 mesh size to be grid independent. The study carried out here revealed that the shift in the reattachment length with changing the grid size and spacings is small compared to the change in other parameters like the mean velocities and the Reynolds stresses at different regions of the domain, making it difficult to ascertain a criterion for grid independency tests. Tahry⁵³ used the Reynolds-Stress Model with a 32 x 30 grid to predict flow in an engine cylinder and observed a shift in the mean velocity profiles at 144°ATDC

when a 45 x 45 grid was employed. According to Armaly et al.⁶ the required grid number to ensure grid independence and the number of iterations (for the same grid number) increases with the Reynolds number. They could not attain complete grid independence with a grid number of 2600 (51 x 51 grid). Likewise Chieng¹³ observed a marked improvement in the Nusselt number predictions for flow into a pipe with a sudden expansion when the grid was changed from 22 x 22 to 50 x 50.

In order to determine a reliable grid system, the grid size was kept fixed at 52 x 52 and exploratory tests were carried out with different grid spacings and lengths of the solution domain. Streamwise mean velocity and Reynolds stress profiles were compared with the experimental data for that particular set of experimental flow conditions. The combination of the grid parameters which had the best agreement was selected to be the final grid system for that particular set of experimental flow conditions. Specific grid details will be mentioned in Chapter 4 while comparing the results of the computation with experimental data.

b) Convergence Criterion.

After having specified the grid system, the cell dimensions and distances are evaluated in the computer program. Initial values of the parameters are then prescribed prior to starting the iteration process.

The convergence criterion of the solution is based on the conservation of mass and momentum in the flow domain. Formulation of equation (3.1.2) for the mean streamwise and transverse velocity components expresses the momentum balance in the flow domain. Satisfaction of these equations upto 1% of the total momentum inflow at the inlet of the channel, constitutes the criterion for convergence. Likewise, formulation of equation (3.1.2) for pressure, expresses the mass balance

in the flow domain. Satisfaction of this equation upto 1% of the total mass inflow at the inlet of the channel, also constitutes the criterion for convergence. The total absolute residual source values for each of these equations is monitored for every iteration and the satisfaction of the above three criterion is taken to be the completion of convergence.

In the solution of the transport equations of the third moments, the total residual source terms for each equation are normalized by $\Sigma \rho A U_{IN}^4$ across the inlet, and are monitored for each iteration. Convergence of the solution for $\overline{u_i u_j u_k}$ is assumed to be completed if either the normalized maximum total residual source is less than 5.0×10^{-12} or if the maximum difference between the residual source terms of two consecutive iterations is less than 3.0×10^{-12} .

In the solution of equations of the RSM incorporating the third moments, the above mentioned convergence criterion needs to be satisfied to qualify for the completion of convergence. However, the consolidation of the RSM by incorporating the transport equations of the third moments requires a large amount of computations. In order to conserve computational time, the convergence criteria for the third moments is made less stringent by relaxing the above mentioned limits to 1.0×10^{-10} and 1.0×10^{-12} , respectively.

c) Model Sequencing

The strong nonlinearity of the system of the equations makes this solution sometimes unstable and hence, susceptible to divergence. In order to avoid divergence, the new models developed in the study are introduced into the solution in sequence.

The solution is begun with the standard k- ϵ model. When the absolute residual source values drop down to about 3%, the Reynolds-Stress Model is invoked which entails the solution of the transport equations of $\overline{u_i u_j}$ along with the momentum and k- ϵ equations iteratively.

In the next sequence, the modified k and ϵ equations are exchanged with the original version when the source term is down to about 2%. The third order closure is introduced in the final sequence when the source term is 1.5%. Convergence is assumed to be complete when the absolute residual source term drops down to 1% and when the source terms for $\overline{u_i u_j u_k}$ have met their convergence criterion. By sequencing the solution of the equations (models) the solution process became less prone to divergence.

Specific grid and model sequencing details are mentioned in Chapter 4 while comparing the computational results with experimental data. The computations were carried out using a UNIVAC 1100 computer. The CPU time and iteration number/history details vary with the turbulence models and with the input data, and are hence mentioned in Chapter 4 along with the specific grid and model sequencing details.

CHAPTER 4

RESULTS AND DISCUSSION OF COMPUTATIONS IN BACKWARD-FACING STEP FLOWS

4.1 Introduction

This chapter presents the results of the study performed in mathematically modeling the turbulence phenomena of separating and reattaching flows. The models developed and presented in Chapter 2 are applied to plane backward-facing step flows and are compared with existing experimental data.

As mentioned earlier, the reason for selecting backward-facing step flows to test the models is that this class of flows possesses most of the important features of flow separation and reattachment. They are greatly susceptible to modeling modifications but, on account of their simple geometry, they are easier to program and compute. Moreover, there exist considerably large sets of reliable and recent data on this class of flows which facilitates better comparison with the modifications in modeling.

In the previous paper⁵, the results obtained with the RSM by solving the transport equations of $\overline{u_i u_j}$, equation (2.1.5), were compared with the results obtained by the $k-\epsilon$ model, in which the Boussinesq correlation, equation (2.1.1), is used to evaluate the Reynolds stresses. Comparison was also made with the computed results of Sindir⁵⁰ using the Algebraic Stress Model (ASM)[§] and the experimental

[§]The ASM was developed by Rodi⁴³ by relating the convective and diffusive transport of the Reynolds stresses to the turbulent kinetic energy k , which after simplification and rearrangement reduce to a set of algebraic equations for evaluating the stresses $\overline{u_i u_j}$.

data of Seegmiller and Driver⁴⁷ and Kim et al.³² who had employed a laser doppler velocimeter (LDV) and hot wire anemometer, respectively, to acquire their data.

Regarding agreement with the experimental data, the results obtained by the RSM showed the best agreement in the recirculating region for predicting normal stresses and showed the best agreement in the reattachment region for predicting shear stresses.

In general, it was found that the $k-\epsilon$ model underpredicts whereas the ASM tends to overpredict the levels of the shear and normal stresses. The results of RSM, however, tend to remain in between the results obtained by the $k-\epsilon$ model and the ASM.

4.2 Transport Equations for Third Moments of Turbulence with Low-Reynolds Number Model

Third moments evaluated by solving the transport equations of $\overline{u_i u_j u_k}$ are compared with the experimental data of Driver and Seegmiller^{19,20} and Chandrsuda and Bradshaw.¹²

After obtaining a good agreement with the experimental data in consideration, the final converged values of the mean velocities, Reynolds stresses, k and ϵ are stored and are used later to solve the transport equation for $\overline{u_i u_j u_k}$ iteratively.

In the high-Reynolds number model of the transport equation for $\overline{u_i u_j u_k}$, the value of the empirical constant C_γ for the pressure-stress effects θ_{ijk} , in equation (2.3.10) is recommended to be 5.8, after matching the peak values of the third moments with experimental data.

In the low-Reynolds number model, the values of the empirical constants C_γ and $C_{\gamma w}$ for the combined effects of the pressure-stress

effect and the near-wall effect, $\theta_{ijk} + \theta_{ijkw}$, were suitably modified and were set equal to 2.0 and 8.0, respectively.

However, in solving the transport equations by both the high-as well as the low-Reynolds number models the effects due to the dissipation rate, ϵ_{ijk} , defined by equation (2.3.12) have not been incorporated for the results presented in this section. This is because the results presented in this section are for reference only. The final results presented in the subsequent section have been obtained by the consolidation of the RSM and contain all the effects discussed earlier.

Figures 4.1 and 4.2 show the computed results of the third moments obtained by both high-and low-Reynolds number models of the transport equation and compare them with the two sets of experimental data mentioned earlier. It is seen that both the high and low-Reynolds number models give similar levels except near the wall, wherein the results obtained by the low-Reynolds number model are improved and are considerably superior. As discussed earlier, the reason for this improvement is attributed to the enhancement of the diffusive transport in the near-wall viscous region due to the additional dissipative effects.

Figures 4.3 and 4.4 compare the profiles of the third moments obtained by the four algebraic models (equations (2.5.2), (2.5.3), (2.5.4), and (2.5.5)) and by those obtained through the solution of the transport equations, incorporating the low-Reynolds number model, with the experimental data. As shown in these figures, the results by the transport equations for the triple velocity correlation give a much better agreement with the experimental data than the results obtained by the corresponding algebraic models. The transport model also improves the prediction near the wall.

The transport model for the third moments is very versatile in its application; its predictions are reliable in both homogeneous and inhomogeneous flows on account of its symmetry property in all the three directions.

The values of the empirical constants, C_γ and $C_{\gamma w}$ were modified slightly after the incorporation of the dissipation term ϵ_{ijk} and after merging the transport equation model for $\overline{u_i u_j u_k}$ with the RSM. Details of this follow in the next section.

4.3 Consolidation of RSM

Results of the third moments presented so far had been obtained implicitly by retrieving and using the converged and stored values of the various parameters to solve the equations for $\overline{u_i u_j u_k}$ iteratively without resolving the equations of those other parameters.

In the consolidation of the Reynolds-Stress Model, however, the transport equation for all the parameters like U and V velocities, k, ϵ , $\overline{u_i u_j}$ and the third moments, $\overline{u_i u_j u_k}$, are solved together iteratively. This system of equations thus involves the iterative solution of a total of 11 equations all of which are nonlinear and intercoupled.

As mentioned in the preceding section (4.2), the values of the empirical constants C_γ and $C_{\gamma w}$ had to be suitably modified during the consolidation of RSM in order to comply with the new system of equations. The final recommended values of these constants are 3.0 and 8.0, respectively.

The solution is initially begun by solving the momentum equations with the original k and ϵ equations (equation (2.2.5) and (2.2.6)). Model sequencing is employed to introduce the new equations into the solution stream.

When the absolute residual source term reaches 3%, the transport equations for the Reynolds stresses are introduced into the computation stream and the iterative process is continued. At the source term value of 2%, the new equations for k and ϵ with the modified diffusive coefficients (equations (2.2.7) and (2.2.8)) are introduced and iterative process is carried on. At the residual source term value of 1.5%, the transport equations for $\overline{u_i u_j u_k}$, (equation (2.4.1)) are finally merged into the computation stream. Complete convergence is assumed when the absolute residual source term drops to less than 1%. Experimental data of Driver and Seegmiller^{19,20} and Chandrsuda and Bradshaw¹² are compared with computational results obtained by three turbulence models explained hereunder.

Model I is the standard k - ϵ model where the Reynolds stresses are evaluated by using the Boussinesq's approximation. A total of 4 transport equations get solved in this case.

Model II refers to modified k - ϵ model that the Reynolds stresses are obtained by solving the transport equations for $\overline{u_i u_j}$ which contain the algebraic correlation of Daly-Harlow¹⁷ for $\overline{u_i u_j u_k}$. A total of 7 transport equations get solved here.

Model III, however, uses the modified equations for k and ϵ , and solves the transport equations for $\overline{u_i u_j}$ as well as $\overline{u_i u_j u_k}$. A total of 11 transport equations are solved iteratively in this case.

In the following figures, unless specified otherwise, the following legend is to be used to identify the models.

<u>Model</u>	<u>Line Type</u>
.....	Model I
-----	Model II
————	Model III
○	Experimental Data

Figures 4.5 and 4.6 compare the U velocity profiles obtained by the different models with the two sets of experimental data.

As shown in figure 4.5, the results obtained by Model III are generally closer to the experimental data. The agreement improves in the shear layer and is more encouraging in the redeveloping region. The three models generally give similar results though the agreement is not quite as good with the data in figure 4.6.

The similarity of the results obtained by the three models is attributed to the fact, that in the solution of the momentum equations, the Reynolds-stress terms are being handled through the turbulent viscosity approximation, and so do not appear in those equations explicitly. This is because, due to the greater significance of the momentum equations (mass balance for proper convergence), they tend to be very sensitive to modeling modifications thereby making the solution unstable. In order to overcome this instability and to avoid divergence, the turbulent viscosity (Boussinesq's approximation) is retained in the momentum equations.

Figures 4.7 and 4.8 compare the shear stress, \overline{uv} , profiles. It is seen that for any given axial location, all the three models predict a more or less similar transverse location of the peak values. The levels predicted by Model I are the lowest of all the three models. Model II tends to overpredict in figure 4.7 whereas Model III overpredicts in figure 4.8. It is seen that the predictions by Model III have generally a better agreement with the experimental data.

Figures 4.9 and 4.10 compare the normal stress $\overline{u^2}$ profiles at different axial distances from the step. The predictions by Model I are always lowest whereas Model III predicts the highest values.

Predictions by Model II seem to give a better agreement with the experimental data.

Figures 4.11 and 4.12 compare the normal stress $\overline{v^2}$ profiles at different axial distances from the step. It is seen that Model I exhibits an opposite trend when predicting the normal stresses $\overline{u^2}$ and $\overline{v^2}$. Model I predicts the largest values whereas Model II predicts the lowest values. The agreement with the experimental data in and around the recirculation region is better with Model III.

Figure 4.13 compares the profiles of the kinetic energy k obtained by different models. Experimental values of the kinetic energy have been obtained by multiplying the sum of the normal stresses ($\overline{u^2}$ and $\overline{v^2}$) by 0.75. It is seen that Model III gives the best predictions with the experimental data whereas Model I is quite deficient in its predictions. The improvement made in the RSM due to the incorporation of the transport equations of the third moments and the modified equations of k and ϵ seems to be encouraging from this figure.

Figure 4.14 compares the energy dissipation rate profiles. Model I seems to give a better agreement whereas Model II is not quite as good. Predictions by Model III are intermediate.

Success in predicting the trends of the various parameters discussed above not only depends upon the type of model being employed but also upon the particular parameter being considered and the location inside the flow domain.

The choice of models had very little influence on predicting the mean velocity profiles. In predicting the Reynolds stresses, however, Model III gave superior results in and around the reattachment region. Model I seemed to give better predictions for $\overline{v^2}$ and energy dissipation rate profiles. Results obtained by Model II seemed to be closer to the results by Model III and generally were better than those by Model I.

Figures 4.15 through 4.21 show the profiles of the various components of the third moments at different axial locations from the step obtained by Models II and III.

Profiles obtained by Model III are consistently superior to those obtained by Model II. The discrepancy with the experimental data is rather large for the profiles of $\overline{v'v'v'}$; both the models underpredict the levels considerably although Model III is still better than Model II.

As discussed earlier, the solution of the complete transport equations of the third moments entails taking into consideration, the phenomena of convection, diffusion, generation, redistribution and dissipation which consequently yields greater accuracy in the turbulence model.

Table 4.1: Computational Details

MODEL	EQUATIONS BEING SOLVED	Computational Details			
		Driver and Seegmiller ¹⁹ (Yo/H = 8.0)		Chandrsuda and Bradshaw ¹² (Yo/H = 2.5)	
		Iteration Number	CPU Time (mins)	Iteration Number	CPU Time (mins)
I	2.1.2 2.2.5 2.2.6	265	25	500	36
II	2.1.2 2.2.5 2.2.6 2.1.15	222	28	443	42
III	2.1.2 2.2.7 2.2.8 2.1.15 2.4.1	240	46	603	72

CHAPTER 5

CONCLUDING REMARKS

The salient feature of this study lies in the fact that it has taken the Reynolds Stress Model of turbulence to a higher degree of sophistication and accuracy through the development and subsequent introduction of the transport equations of the third moments into it. Being primary diffusive transporters, the correct simulation of the third moments, thus enables genuine government of the Reynolds stresses in the flow fields with separation, reattachment and recirculation. Inadequacy of the existing algebraic equations for evaluating the third moments was demonstrated, and approximate correction factors were recommended for these equations by comparing them with the experimental data.

Development of the transport equations of third moments required the formulation of their equation and then the modeling of the various terms in the formulated equation which was sometimes attained through the use of empirical constants. The relative effect of the constants on the behavior of the third moments was investigated and suitable values of these constants were recommended.

A low-Reynolds number model was developed and incorporated into the transport equations of the third moments which greatly improved their predictions near the wall.

With regard to the Reynolds stresses, however, the RSM predicted better normal stresses in the recirculating regions and better shear stresses in the reattachment region.

The highlight of this theoretical study is the consolidation of the RSM by merging it with equations of k and ϵ containing the new recommended diffusion coefficients and the transport equations of the third moments containing the low-Reynolds number effect. This system of equations required the iterative solution of 11 non-linear and intercoupled equations. The mean velocity, Reynolds stresses, k , ϵ and third moments profiles thus obtained were compared with two sets of experimental data and with similar computational results obtained by the k - ϵ model and the original RSM.

In the modeling process and the determination of empirical constants the experimental data have been relied on heavily. Since the experimental data are associated with various levels of uncertainties, the corresponding theoretical models are also associated themselves with some of these uncertainties which may be reduced in future studies.

REFERENCES

1. Amano, R. S., Jensen, M. K. and Goel, P., (1983), "A Numerical and Experimental Investigation of Turbulent Heat Transport Downstream from an Abrupt Pipe Expansion," Journal of Heat Transfer, Vol. 105, pp. 862-869.
2. Amano, R. S. and Goel, P., (1983), "Turbulent Heat Transfer in the Separated Reattached and Redevelopment Regions of a Circular Tube," AIAA Paper No. AIAA-83-1520.
3. Amano, R. S. and Goel, P., (1984), "A Numerical Study of a Separating and Reattaching Flow by Using Reynolds-Stress Turbulence Closure," Numerical Heat Transfer, Vol. 7, pp.343-357.
4. Amano, R. S., (1984), "Turbulence Models for Numerical Computations," Class-notes for ME 612-890, Dept. of Mechanical Engineering, University of Wisconsin, Milwaukee.
5. Amano, R. S. and Goel, P., (1985), "Computations of Turbulent Flow Beyond Backward-Facing Steps Using Reynolds-Stress Closure," AIAA Journal, Vol. 23, No. 9, pp. 1356-1361.
6. Armaly, B. F., Durst, F., Pereira, J. C. F. and Schonung, B., (1983), "Experimental and Theoretical Investigation of Backward-Facing Step Flow," Journal of Fluid Mechanics, Vol. 127, pp. 473-496.
7. Bird, R. B., Stewart, W. E., and Lightfoot, E. N., (1960), Transport Phenomena, John Wiley and Sons, Inc.
8. Bradshaw, P., (ed.)(1978), Turbulence-Topics in Applied Physics, Vol. 12, Springer-Verlag.
9. Bradshaw, P. and Wong, F. Y. F., (1972), "The Reattachment and Relaxation of a Turbulent Shear Layer," Journal of Fluid Mechanics, Vol. 52, pp. 113-135.
10. Boyle, D. R. and Golay, M. W., (1983), "Measurement of a Recirculating, Two-Dimensional, Turbulent Flow and Comparison to Turbulence Model Predictions. I: Steady State Case", Journal of Fluids Engineering. Vol. 105, pp. 439-446.
11. Celenligil, M. C. and Mellor, G. L., (1985), "Numerical Solution of Two-Dimensional Turbulent Separated Flows Using a Reynolds Stress Closure Model," ASME Paper No. 85-WA/FE-5.
12. Chandrsuda, C. and Bradshaw, P., (1981), "Turbulence Structure of a Reattaching Mixing Layer," Journal of Fluid Mechanics, Vol. 110, pp. 171-194.
13. Chieng, C. C., (1980), "An Investigation of Turbulence Modeling for the Abrupt Pipe Expansion," ASME Paper No. 83-FE-15.

14. Chieng, C. C. and Launder, B. E., (1980), "On the Calculation of Turbulent Heat Transport Downstream from an Abrupt Pipe Expansion," Numerical Heat Transfer, Vol. 3, pp. 189-207.
15. Chou, P. Y., (1945), "On Velocity Correlations and the Solution of the Equations of Turbulent Fluctuation", Quarterly of Applied Mathematics, Vol. 3, pp. 38-54.
16. Cormack, D. E., Leal, L. G. and Seinfeld, J. H., (1978), "An Evaluation of Mean Reynolds Stress Turbulence Models: The Triple Velocity Correlation," Journal of Fluids Engineering, Vol. 100, pp. 47-54.
17. Daly, B. J. and Harlow, F. H., (1970), "Transport Equations in Turbulence," The Physics of Fluids, Vol. 13, No. 11, pp. 2634-2649.
18. Domaradzki, J. A. and Mellor, G. L., (1984), "A Simple Turbulence Closure Hypothesis for the Triple-Velocity Correlation Functions in Homogeneous Isotropic Turbulence", Journal of Fluid Mechanics, Vol. 140, pp. 45-61.
19. Driver, D. M. and Seegmiller, H. L., (1985), "Features of a Reattaching Turbulent Shear Layer in Divergent Channel Flow," AIAA Journal, Vol. 23, No. 2, pp. 163-171.
20. Driver, D. M., and Seegmiller, H. L., (1985), Private communication.
21. Eaton, J. K. and Johnston, J. P., (1981), "A Review of Research on Subsonic Turbulent Flow Reattachment," AIAA Journal, Vol. 19, No. 9, pp. 1093-1100.
22. Etheridge, D. W. and Kemp, P. H., (1978), "Measurements of Turbulent Flow Downstream of a Rearward-Facing Step," Journal of Fluid Mechanics, Vol. 86, pp. 545-566.
23. Gibson, M. M. and Launder, B. E., (1978), "Ground Effects on Pressure Fluctuations in the Atmospheric Boundary Layer," Journal of Fluid Mechanics, Vol. 86, pp. 491-511.
24. Gosman, A. D. and Ideriah, F. J. K., (1976), "TEACH-T: A General Computer Program for Two-Dimensional, Turbulent, Recirculating Flows," Mechanical Engineering Department Report, Imperial College, London.
25. Hanjalic, K. and Launder, B. E., (1972), "A Reynolds Stress Model of Turbulence and Its Application to Thin Shear Flows," Journal of Fluid Mechanics, Vol. 52, Part 4, pp. 609-638.
26. Hanjalic, K. and Launder, B. E., "Contribution Towards a Reynolds-stress Closure for Low-Reynolds-Number Turbulence," Journal of Fluid Mechanics, Vol. 74, part 4, pp. 593-610.

27. Hanjalic, K. and Launder, B. E., (1972), "Fully Developed Asymmetric Flow in a Plane Channel", Journal of Fluid Mechanics, Vol. 51, part 2, pp. 301-335.
28. Hinze, J. O., (1975), Turbulence, McGraw-Hill.
29. Irwin, H. P. A. H., (1973), "Measurements in a Self-Preserving Plane Wall Jet in a Positive Pressure Gradient," Journal of Fluid Mechanics, Vol. 61, pp. 33-63.
30. Jones, W. P., and Launder, B. E., (1972), "The Prediction of Laminarization with a Two-Equation Model of Turbulence," International Journal of Mass Transfer, Vol. 15, pp. 301-314.
31. Jones, W. P., and Launder, B. E., (1973), "The Calculation of Low-Reynolds-Number Phenomena with a Two-Equation Model of Turbulence," International Journal of Mass Transfer, Vol 16, pp.1119-1130.
32. Kim, J., Kline, S. J. and Johnston, J. P., (1980), "Investigation of a Reattaching Turbulent Shear Layer: Flow Over a Backward-Facing Step," Journal of Fluids Engineering, Vol. 102, pp. 302-308.
33. Launder, B. E. and Spalding, D. B., (1973), Lectures in Mathematical Models of Turbulence", Academic Press.
34. Launder, B. E., Reece, G. J. and Rodi, W., (1975), "Progress in the Development of a Reynolds-Stress Turbulence Closure," Journal of Fluid Mechanics, Vol. 68, pp. 537-566.
35. Launder, B. E., (1975), "On the Effects of a Gravitational Field on the Turbulent Transport of Heat and Momentum," Journal of Fluid Mechanics, Vol. 67, pp. 569-581.
36. Lawn, C. J., (1971), "The Determination of the Rate of Dissipation in Turbulent Pipe Flow," Journal of Fluid Mechanics, Vol. 48., p. 477-501.
37. Lumley, J. L. and Khajeh Nouri, B., (1974), "Computational Modeling of Turbulent Transport, Advances in Geophysics, Vol. 18A, pp. 169-192.
38. Naot, D., Shavit, A., and Wolfshtein, M., (1973), "Two-point Correlation Model and the Redistribution of Reynolds Stresses," Physics of Fluids, Vol. 16, No. 6, pp. 738-743.
39. Nikjooy, M., So, R. M. C., and Hwang, B. C., (1985), "A Comparison of Three Algebraic Stress Closures for Combustor Flow Calculations," ASME Paper No. 85-WA/FE-3.
40. Patankar, S. V., (1980), Numerical Heat Transfer and Fluid Flow, McGraw-Hill.
41. Pope, S. B. and Whitelaw, J. H., (1976), "The Calculation of Near-Wake Flows," Journal of Fluid Mechanics, Vol. 73, pp. 9-32.

42. Roache, P. J., (1976), Computational Fluid Dynamics., Hermosa Publishers.
43. Rodi, W., (1982), "The Prediction of Free Boundary Layers by Use of a Two-Equation Model of Turbulence," Ph.D. Thesis, University of London.
44. Rotta, J. C. (1951), "Statistische Theorie Nichthomogener Turbulenz," Z. Phys., Vol. 129, p. 547.
45. Ruderich, R. and Fernholz, H. H., (1986), "An Experimental Investigation of a Turbulent Shear Flow with Separation, Reverse Flow, and Reattachment," Journal of Fluid Mechanics, Vol. 163, pp. 283-322.
46. Schlichting, H., (1968), Boundary-Layer Theory, McGraw Hill.
47. Seegmiller, H. L. and Driver, D. M., (1984), Private Communication.
48. Shir, C. C., (1973), "A Preliminary Numerical Study of Atmospheric Turbulent Flows in the Idealized Planetary Boundary Layer," Journal of Atmospheric Sciences, Vol. 30, pp. 1327-1339.
49. Simpson, R. L., (1981), "Review - A Review of Some Phenomena in Turbulent Flow Separation," Journal of Fluids Engineering, Vol. 103, pp. 520-533.
50. Sindir, M. M. S., (1982), "A Numerical Study of Turbulent Flows in Backward-Facing Step Geometries: A Comparison of Four Models of Turbulence," Ph.D. Thesis, University of California, Davis.
51. Smyth, R., "Turbulent Flow Over a Plane Symmetric Sudden Expansion," Journal of Fluids Engineering, Vol. 101, pp. 348-353.
52. Stevenson, W. H., Thompson, H. D. and Craig, R. R., (1984) "Laser Velocimeter Measurements in Highly Turbulent Recirculating Flows," Journal of Fluids Engineering, Vol. 106, pp. 173-180.
53. Tahry, S. L., (1985), "Application of a Reynolds Stress Model to Engine-Like Flow Calculations," Journal of Fluids Engineering, Vol. 107, pp. 444-450.
54. Tennekes, H., and Lumley, J. L., (1983), A First Course in Turbulence, The MIT Press.
55. Thompson, B. E. and Whitelaw, J. H., (1985), "Characteristics of a Trailing-Edge Flow with Turbulent Boundary-Layer Separation," Journal of Fluid Mechanics, Vol. 157, pp. 305-326.
56. Walteric, R. E., Jagoda, J. I., Richardson, C. R. J., de Groot, W. A., Strahle, W. C. and Hubbartt, J. E., "Experiments and Computation on Two Dimensional Turbulent Flow Over a Backward Facing Step," AIAA Paper No. AIAA-84-0013.

57. Weinstock, J., and Burk, S., (1985), "Theoretical Pressure-Strain Terms, Experimental Comparison, and Resistance to Large Anisotropy," Journal of Fluid Mechanics, Vol. 154, pp. 429-443.
58. Wynanski, I. and Fiedler, H. E., (1970), "The Two-Dimensional Mixing Region," Journal of Fluid Mechanics, Vol. 41, pp. 327-361.

LIST OF FIGURES

- FIGURE 1.1 Backward-facing flow geometry with the separating, recirculation and redeveloping regions
- FIGURE 2.1 Variation of energy dissipation rate with non-dimensional distance from the wall
- FIGURE 3.1 Node P with neighboring nodes and fluxes at the control surfaces
- FIGURE 3.2 Staggered grid system for the evaluation of the mean velocities, Reynolds stresses and the third moments.
- FIGURE 4.1 Third moments obtained by the transport equations with the high and low-Reynolds number models
- FIGURE 4.2 Third moments obtained by the transport equations with the high and low-Reynolds number models
- FIGURE 4.3 Third moments obtained by the original algebraic correlations and the transport equations incorporating the low-Reynolds number model
- FIGURE 4.4 Third moments obtained by the original algebraic correlations and the transport equations incorporating the low-Reynolds number model
- FIGURE 4.5 U-velocity profiles behind the step. Comparison with data of Driver and Seegmiller
- FIGURE 4.6 U-velocity profiles behind the step. Comparison with data of Chandrsuda and Bradshaw
- FIGURE 4.7 \overline{uv} -profiles behind the step. Comparison with data of Driver and Seegmiller
- FIGURE 4.8 \overline{uv} -profiles behind the step. Comparison with data of Chandrsuda and Bradshaw
- FIGURE 4.9 $\overline{u^2}$ -profiles behind the step. Comparison with data of Driver and Seegmiller
- FIGURE 4.10 $\overline{u^2}$ -profiles behind the step. Comparison with data of Chandrsuda and Bradshaw
- FIGURE 4.11 $\overline{v^2}$ -profiles behind the step. Comparison with data of Driver and Seegmiller
- FIGURE 4.12 $\overline{v^2}$ -profiles behind the step. Comparison with data of Chandrsuda and Bradshaw
- FIGURE 4.13 k-profiles behind the step. Comparison with data of Driver and Seegmiller

- FIGURE 4.14 ϵ -profiles behind the step. Comparison with data of Driver and Seegmiller
- FIGURE 4.15 \overline{uuu} -profiles behind the step. Comparison with data of Driver and Seegmiller
- FIGURE 4.16 \overline{uuv} -profiles behind the step. Comparison with data of Driver and Seegmiller
- FIGURE 4.17 \overline{uvv} -profiles behind the step. Comparison with data of Chandrsuda and Bradshaw
- FIGURE 4.18 \overline{uvv} -profiles behind the step. Comparison with data of Driver and Seegmiller
- FIGURE 4.19 \overline{uvv} -profiles behind the step. Comparison with data of Chandrsuda and Bradshaw
- FIGURE 4.20 \overline{vvv} -profiles behind the step. Comparison with data of Driver and Seegmiller
- FIGURE 4.21 \overline{vvv} -profiles behind the step. Comparison with data of Chandrsuda and Bradshaw

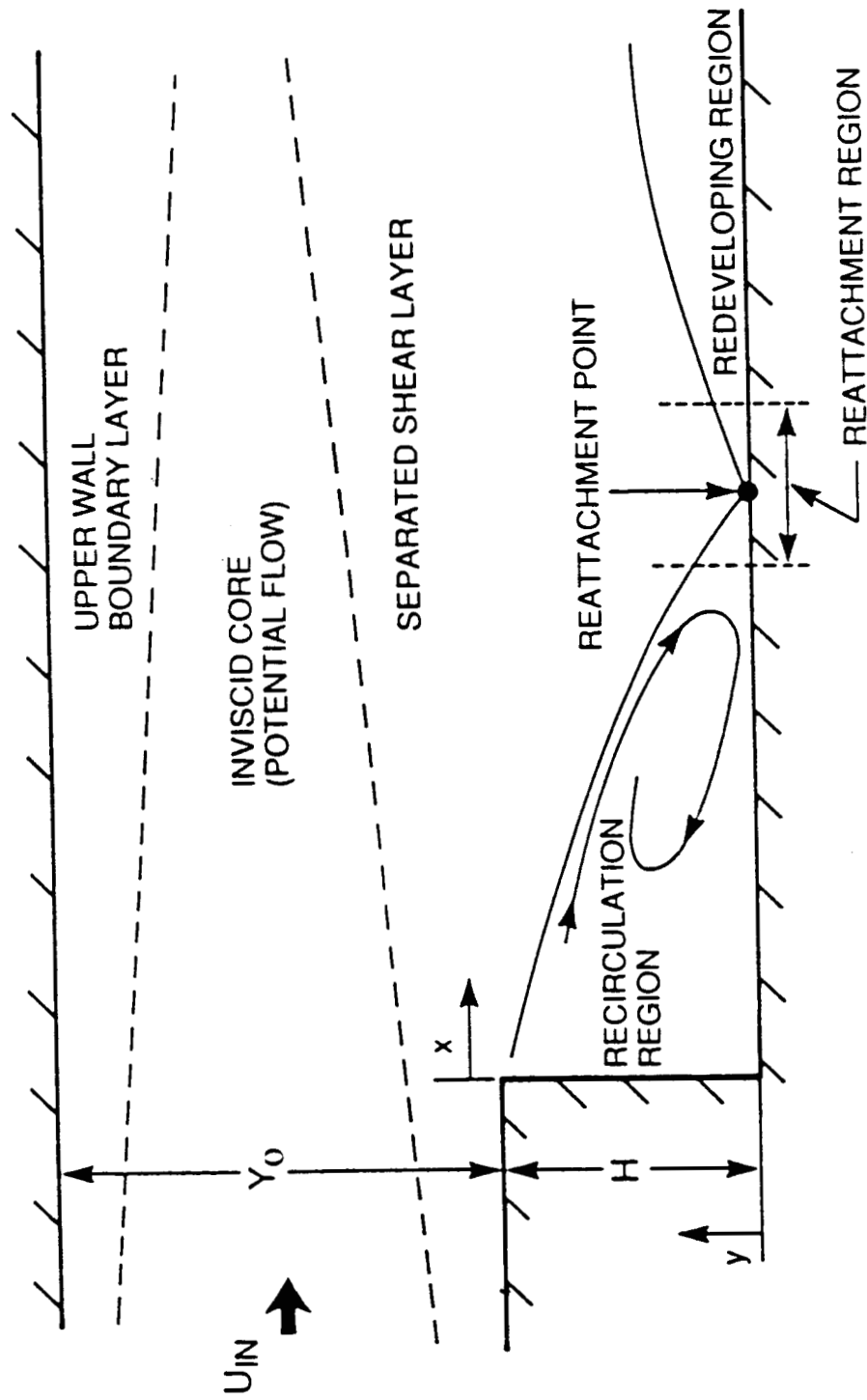


FIGURE 1.1 Backward-facing flow geometry with the separating, recirculation and redeveloping regions

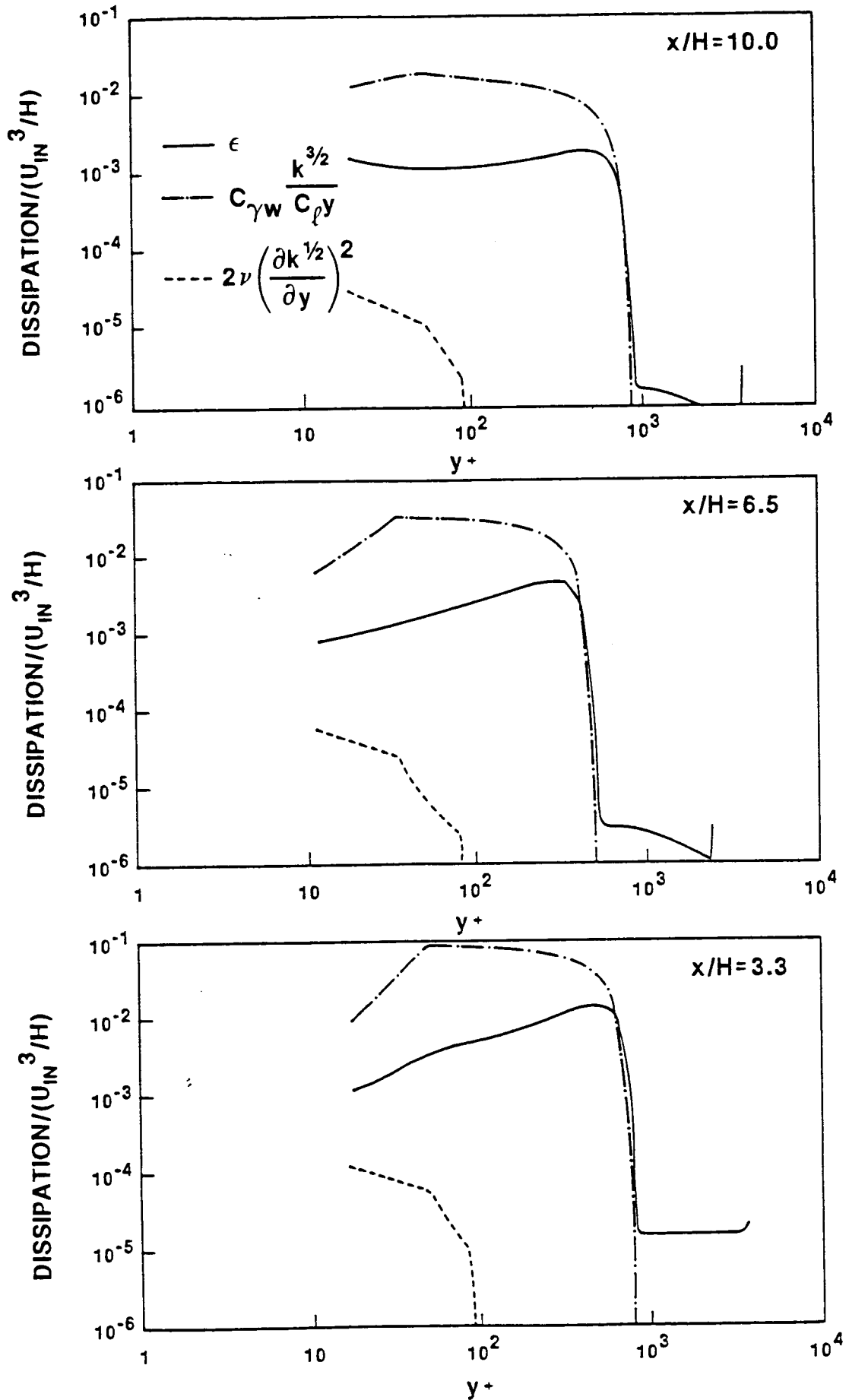


FIGURE 2.1 Variation of energy dissipation rate with non-dimensional distance from the wall

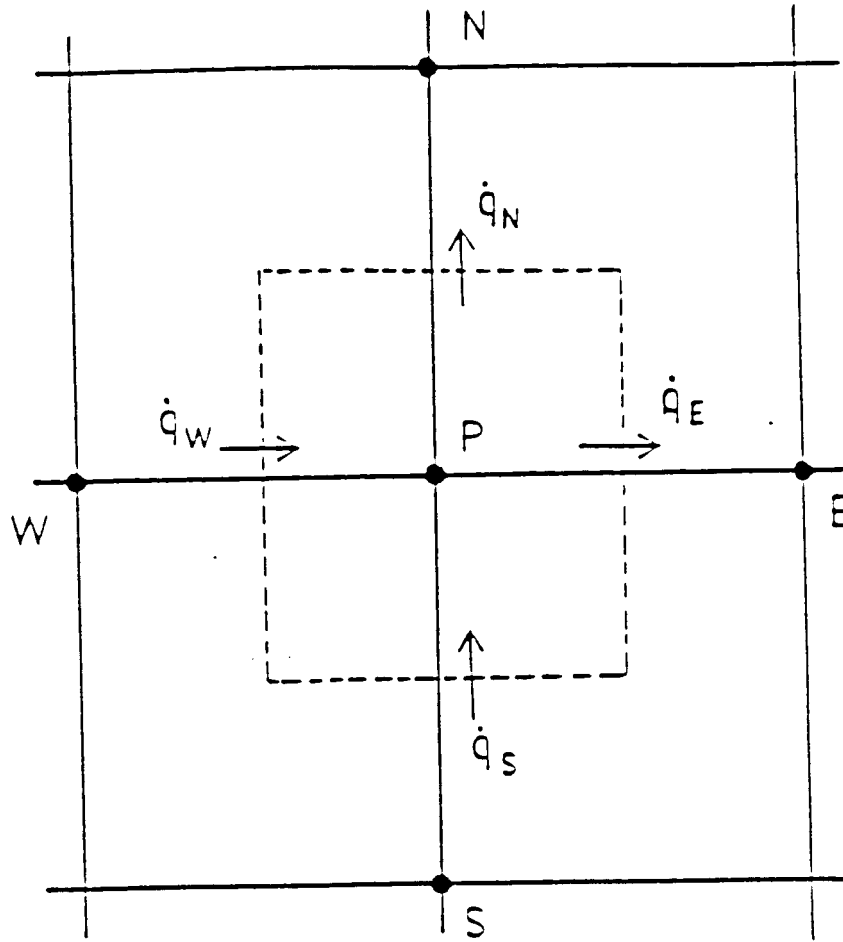


FIGURE 3.1 Node P with neighboring nodes and fluxes at the control surfaces

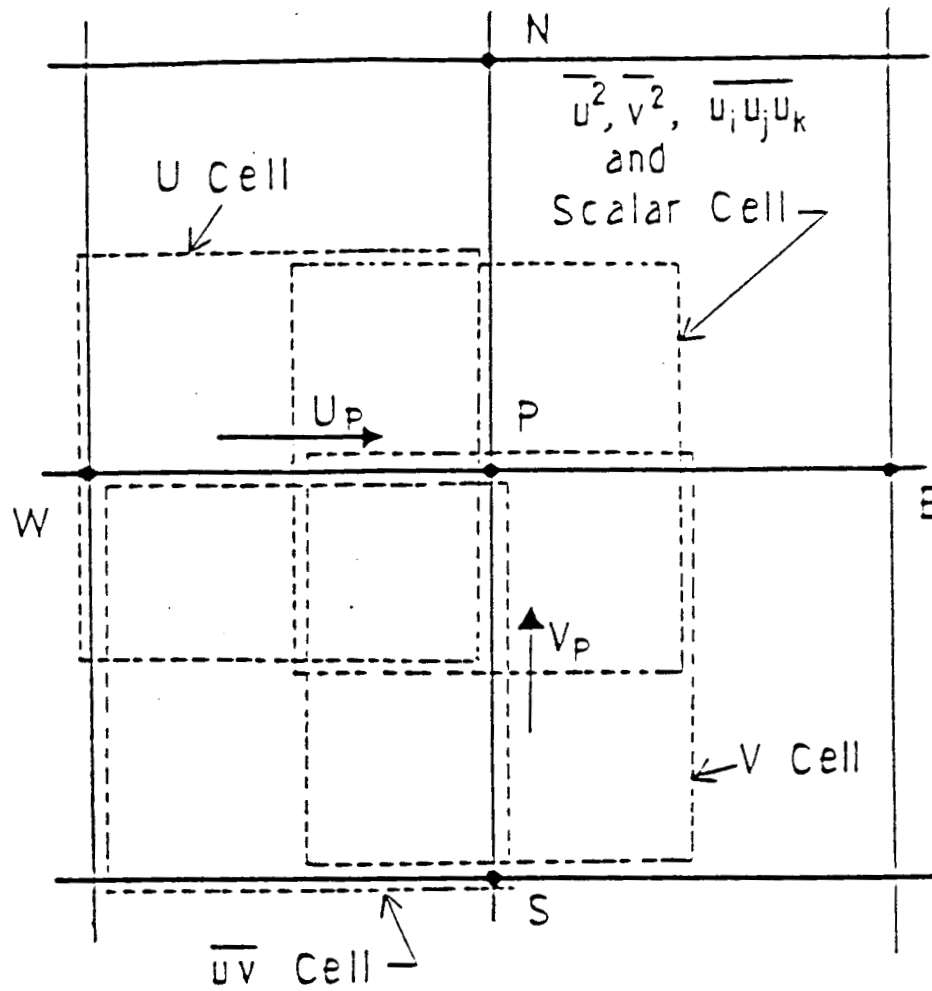


FIGURE 3.2 Staggered grid system for the evaluation of the mean velocities, Reynolds stresses and the third moments.

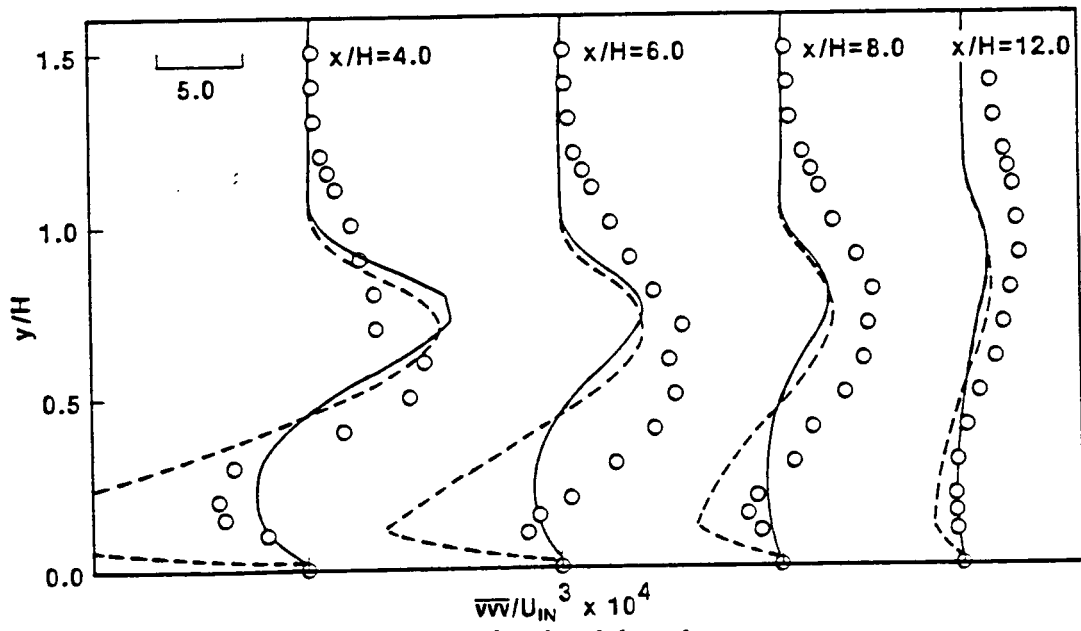
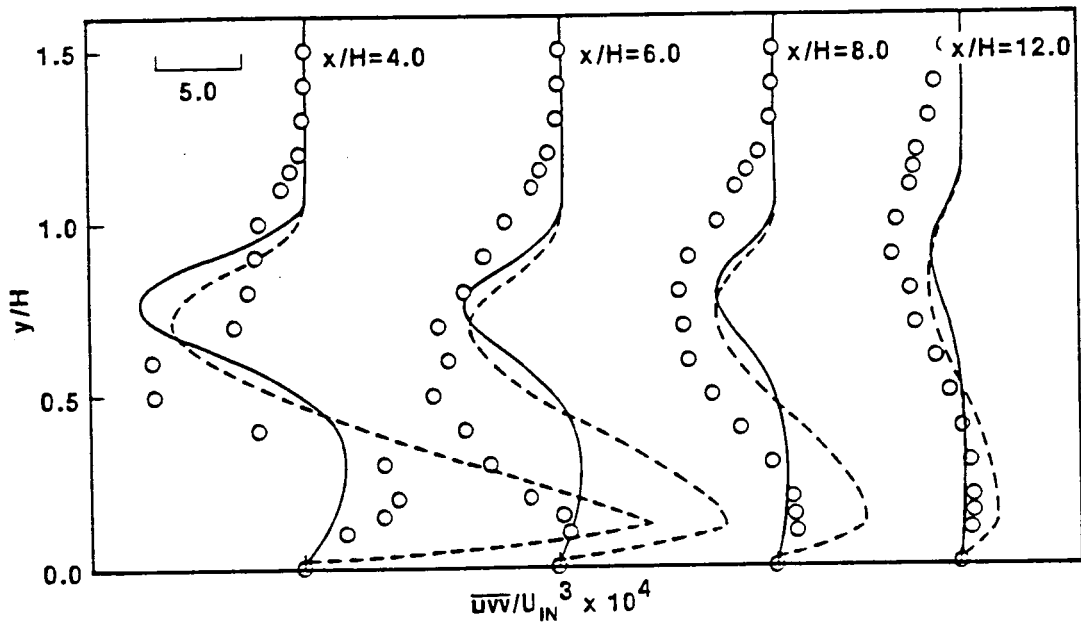
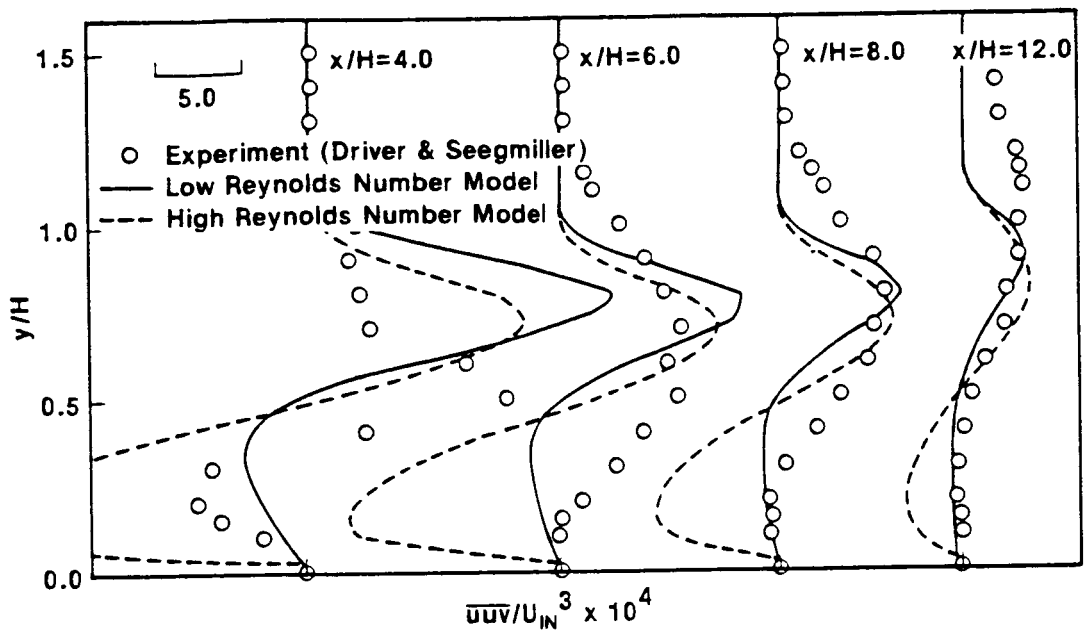


FIGURE 4.1 Third moments obtained by the transport equations with the high and low-Reynolds number models

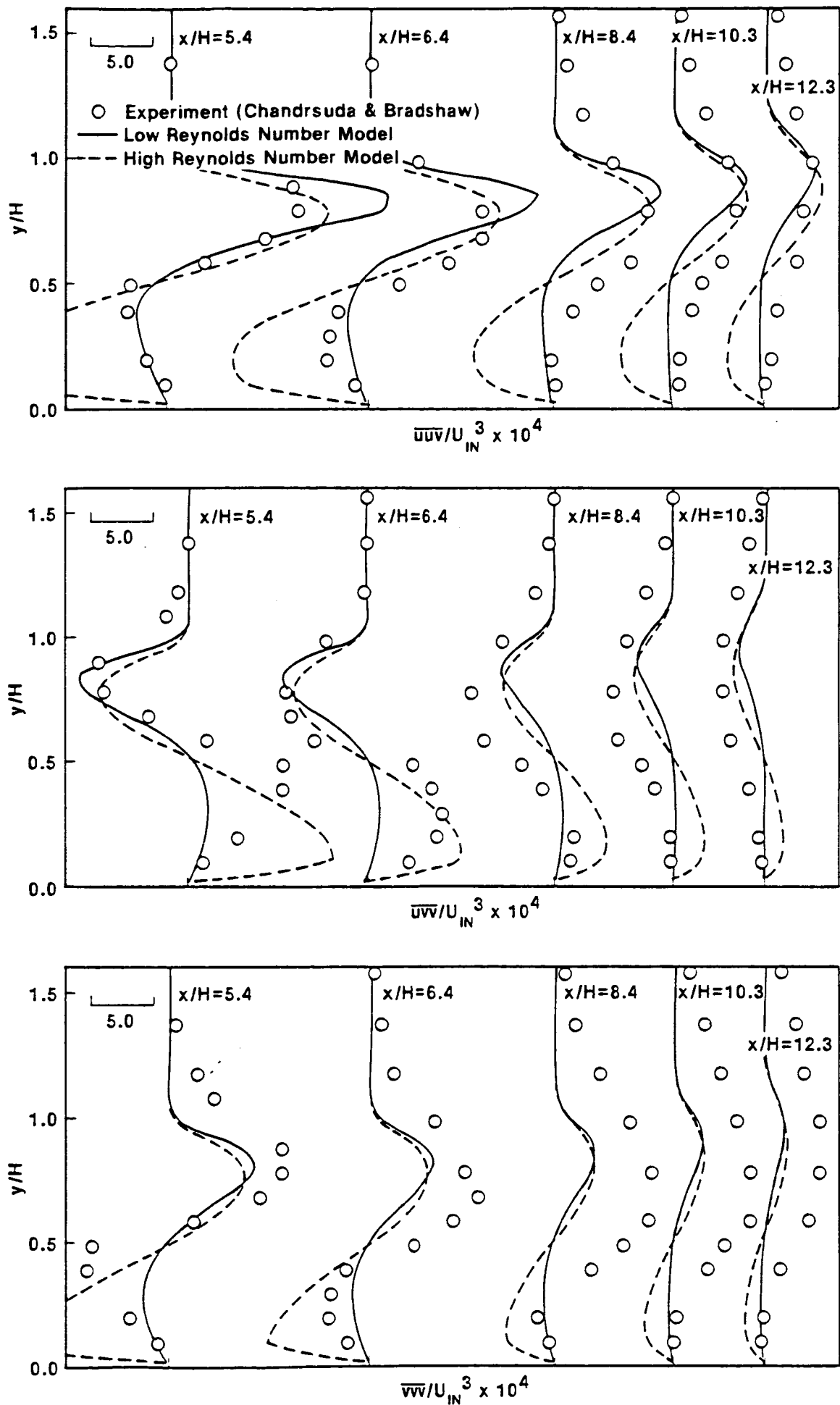


FIGURE 4.2 Third moments obtained by the transport equations with the high and low-Reynolds number models

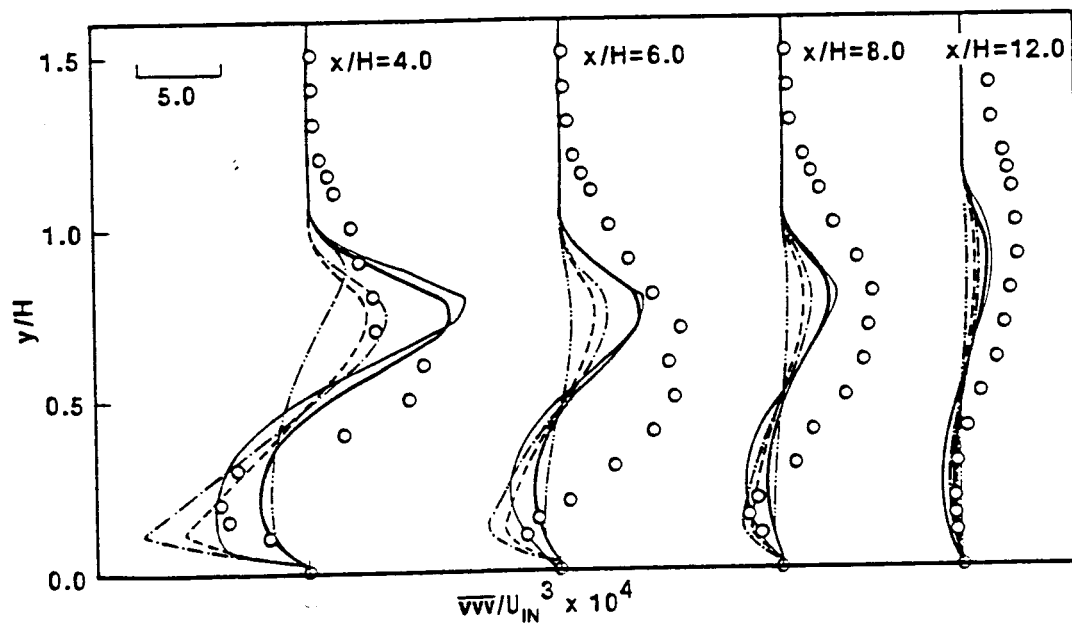
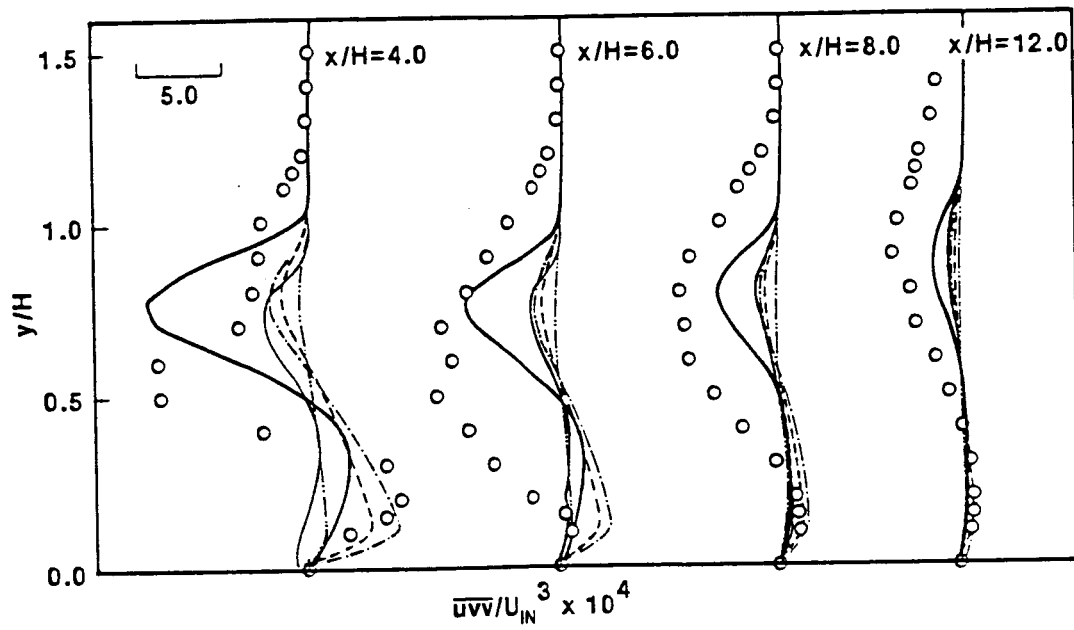
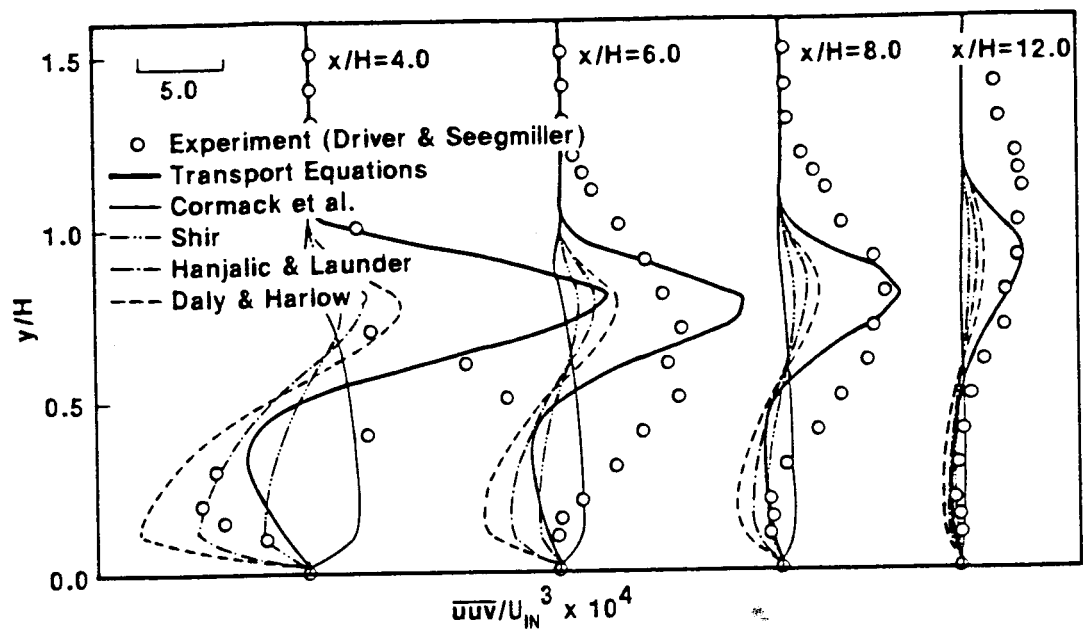


FIGURE 4.3 Third moments obtained by the original algebraic correlations and the transport equations

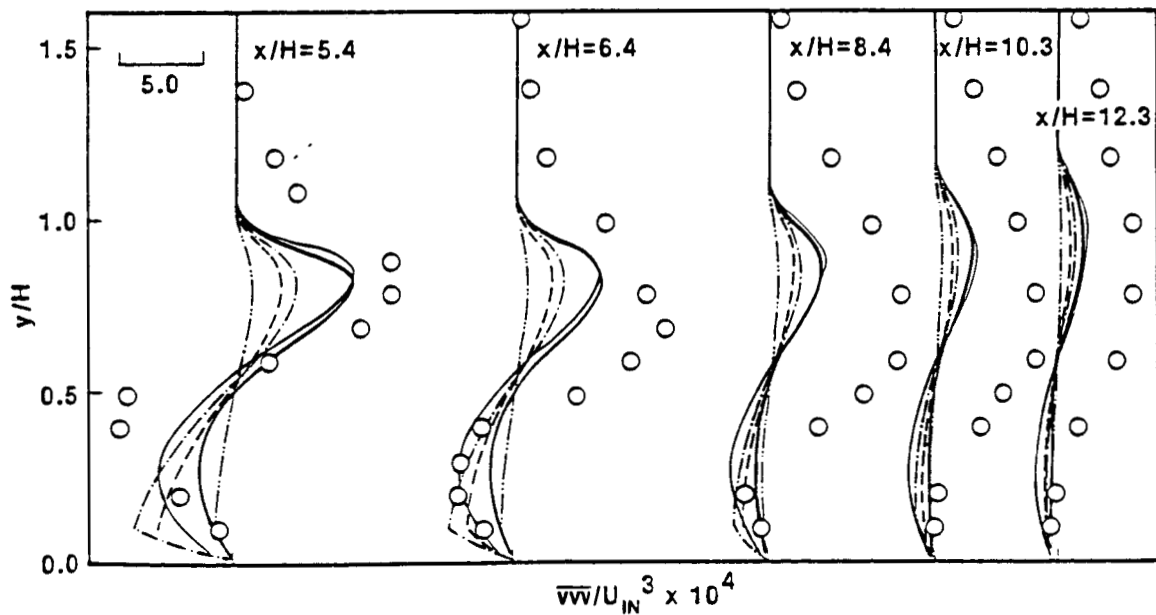
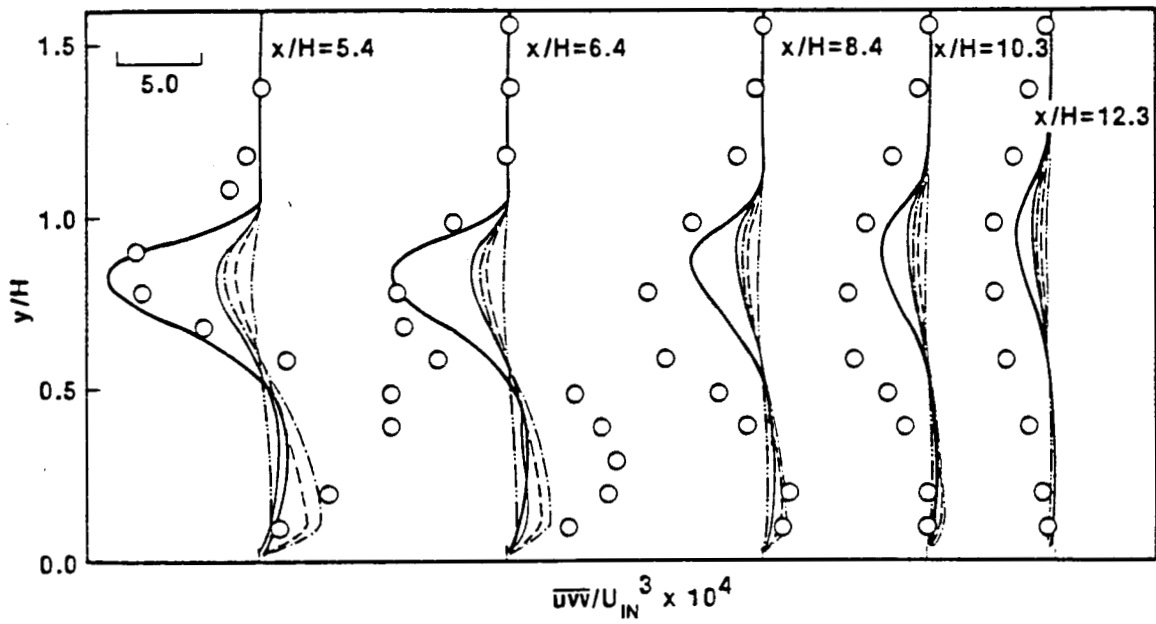
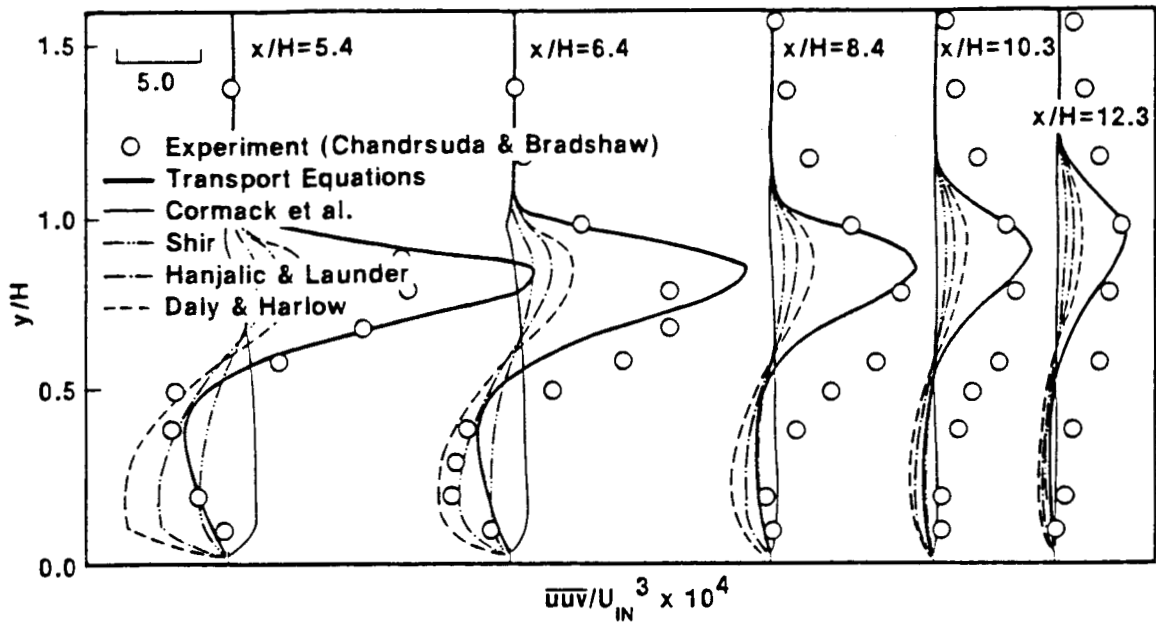


FIGURE 4.4 Third moments obtained by the original algebraic correlations and the transport equations

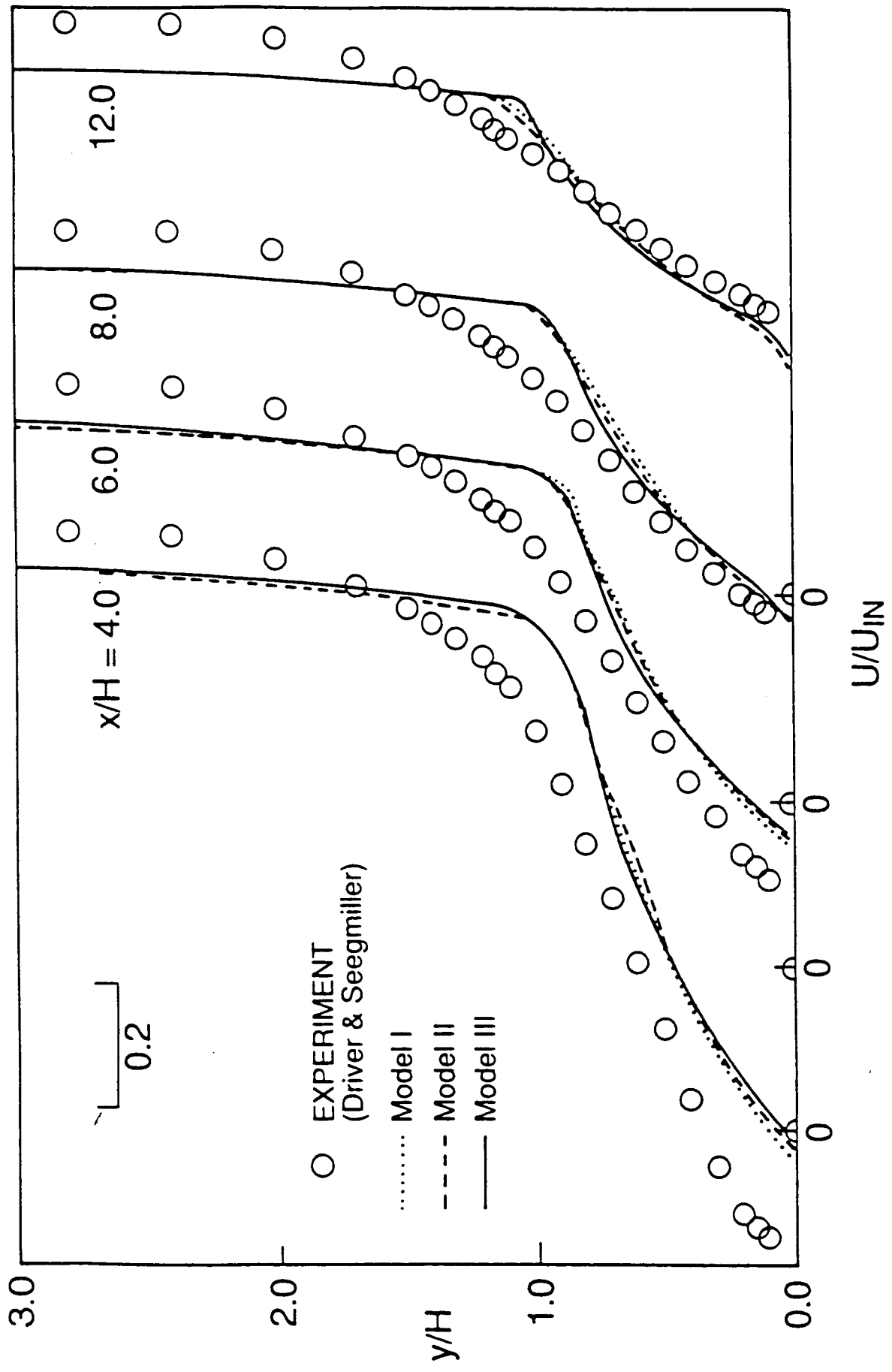


FIGURE 4.5 U-velocity profiles behind the step. Comparison with data of Driver and Seegmiller

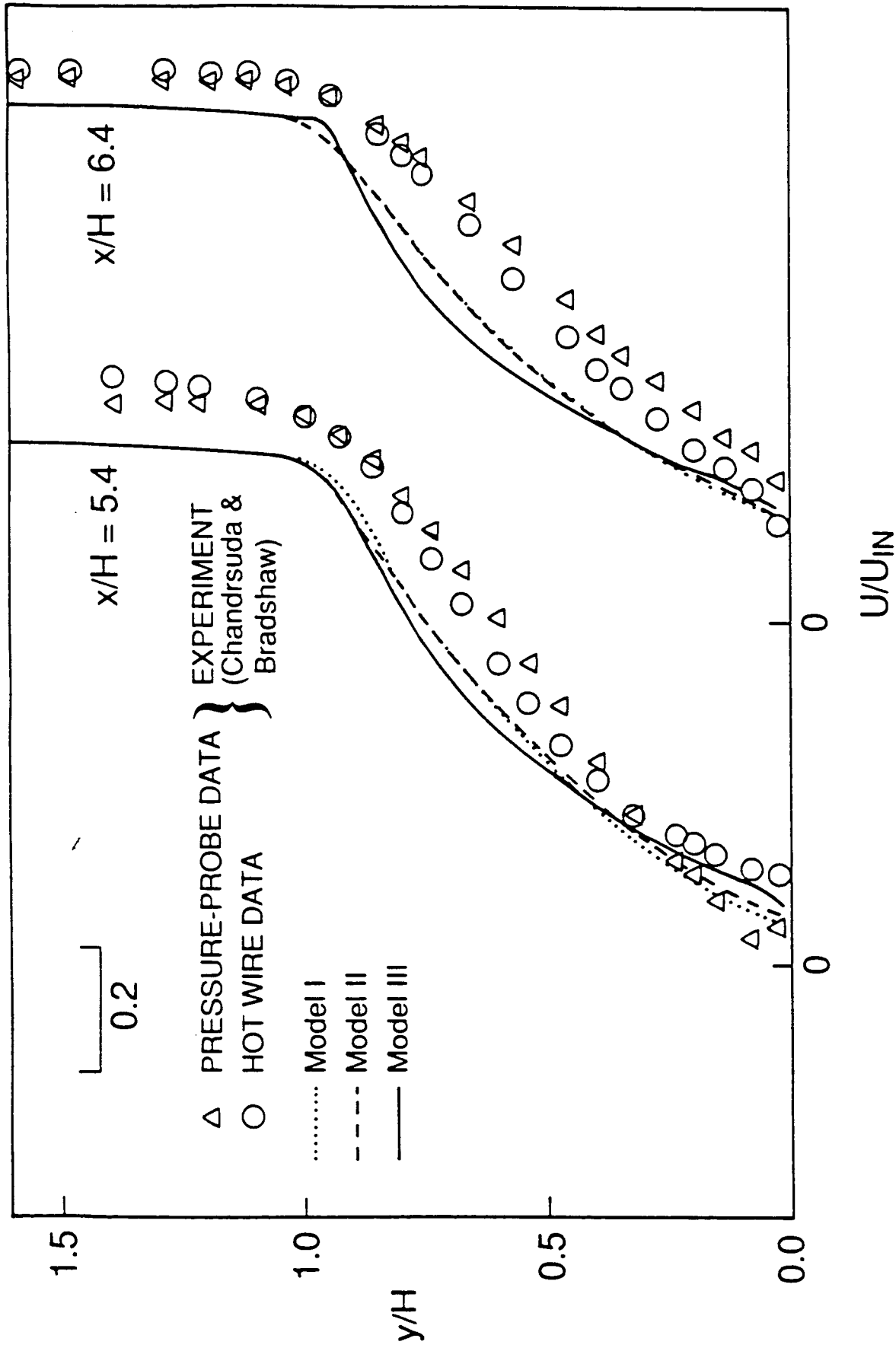


FIGURE 4.6 U-velocity profiles behind the step. Comparison with data of Chandrusuda and Bradshaw

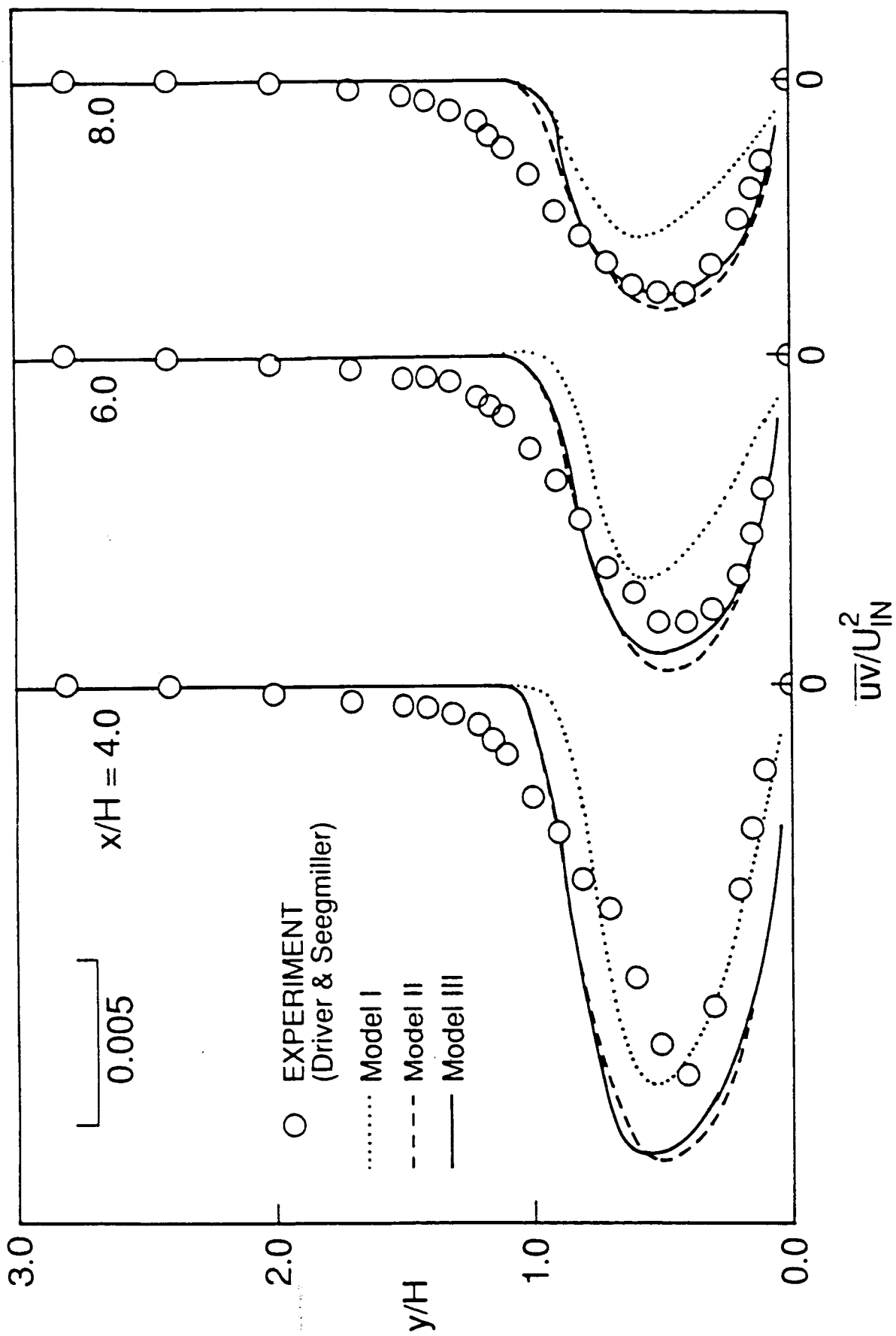


FIGURE 4.7 \overline{uv} -profiles behind the step. Comparison with data of Driver and Seegmiller

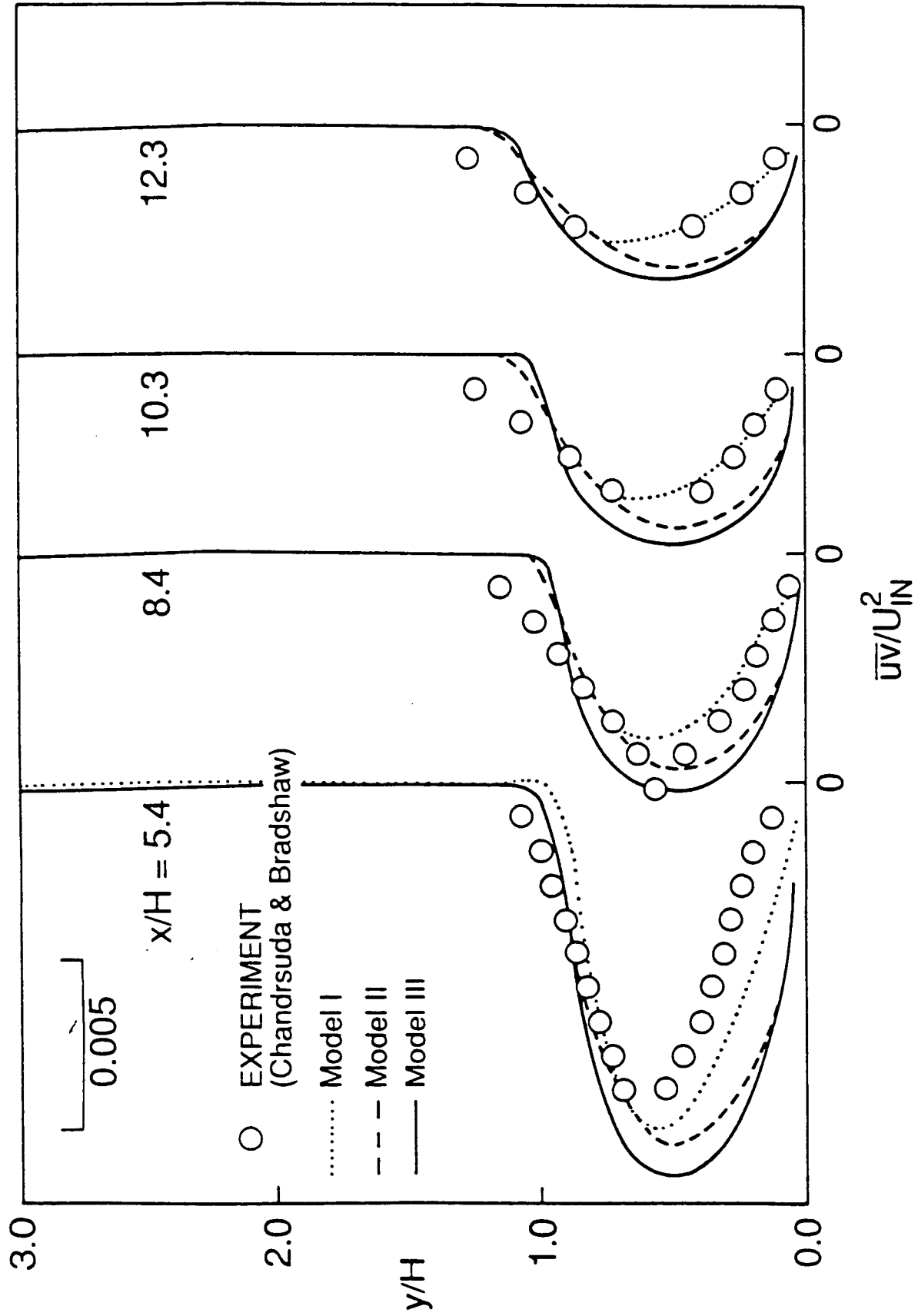


FIGURE 4.8 \overline{uv} -profiles behind the step. Comparison with data of Chandrsuda and Bradshaw

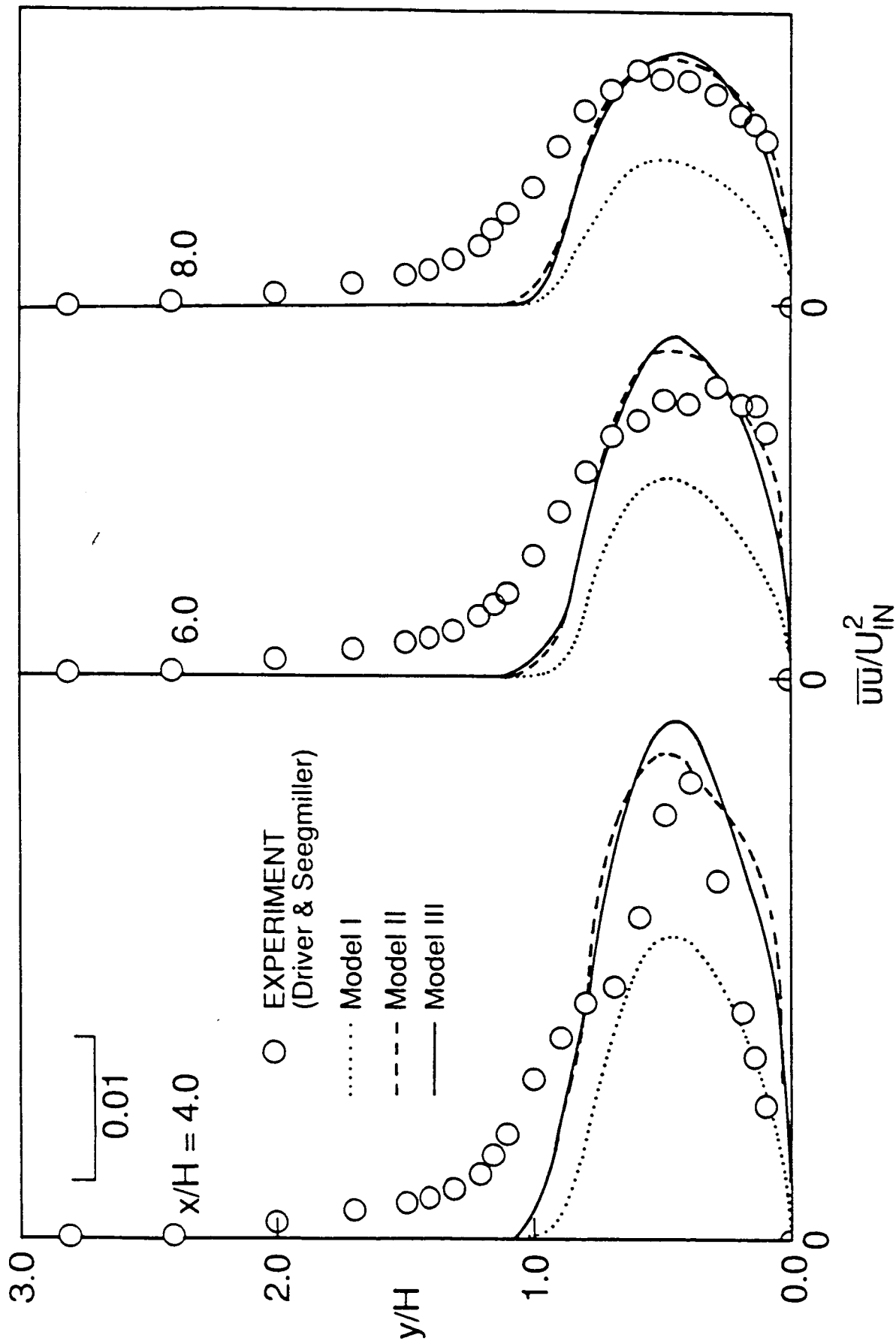


FIGURE 4.9 $\overline{u^2}$ -profiles behind the step. Comparison with data of Driver and Seegmiller

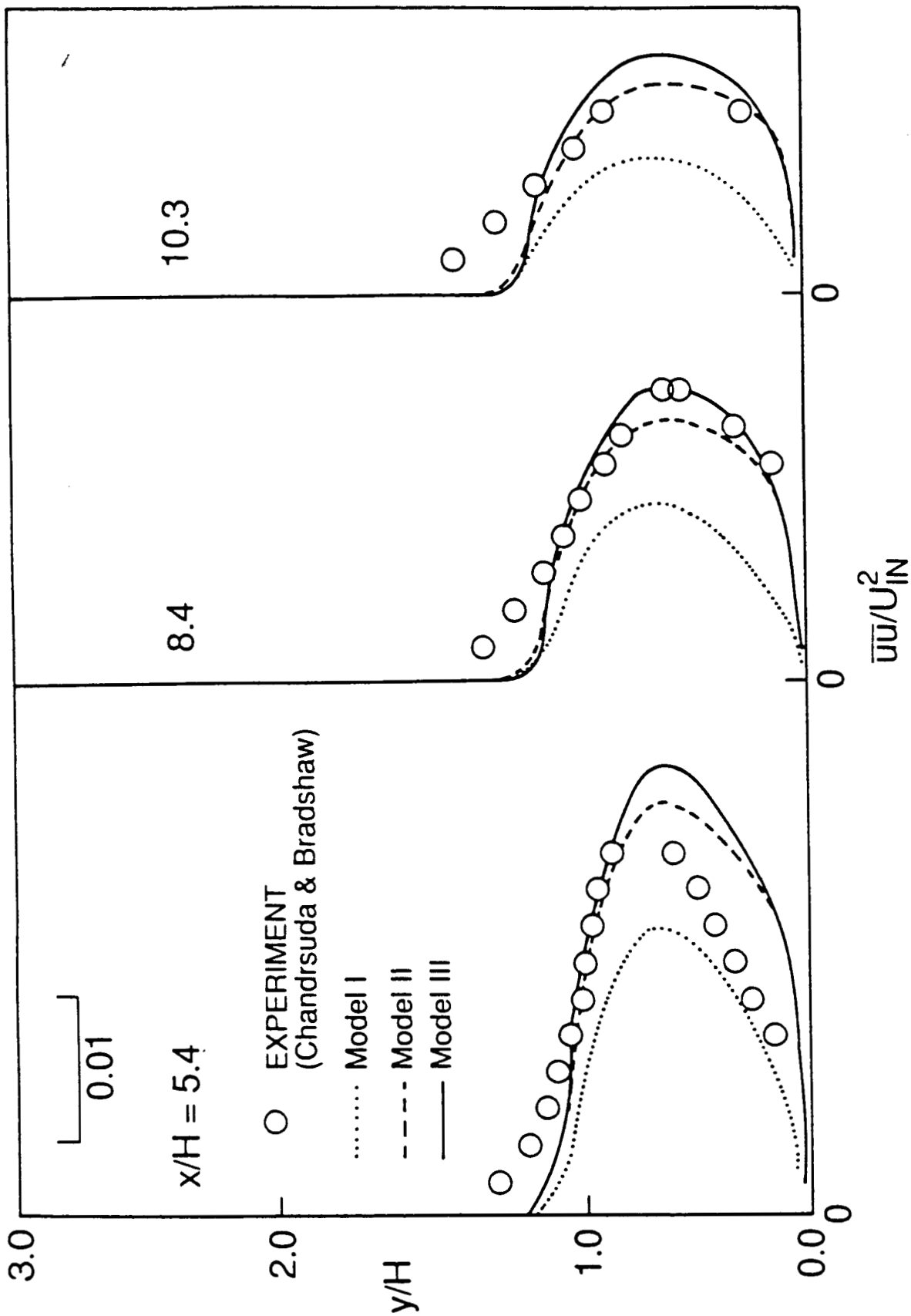


FIGURE 4.10 $\overline{u^2}$ -profiles behind the step. Comparison with data of Chandrsuda and Bradshaw

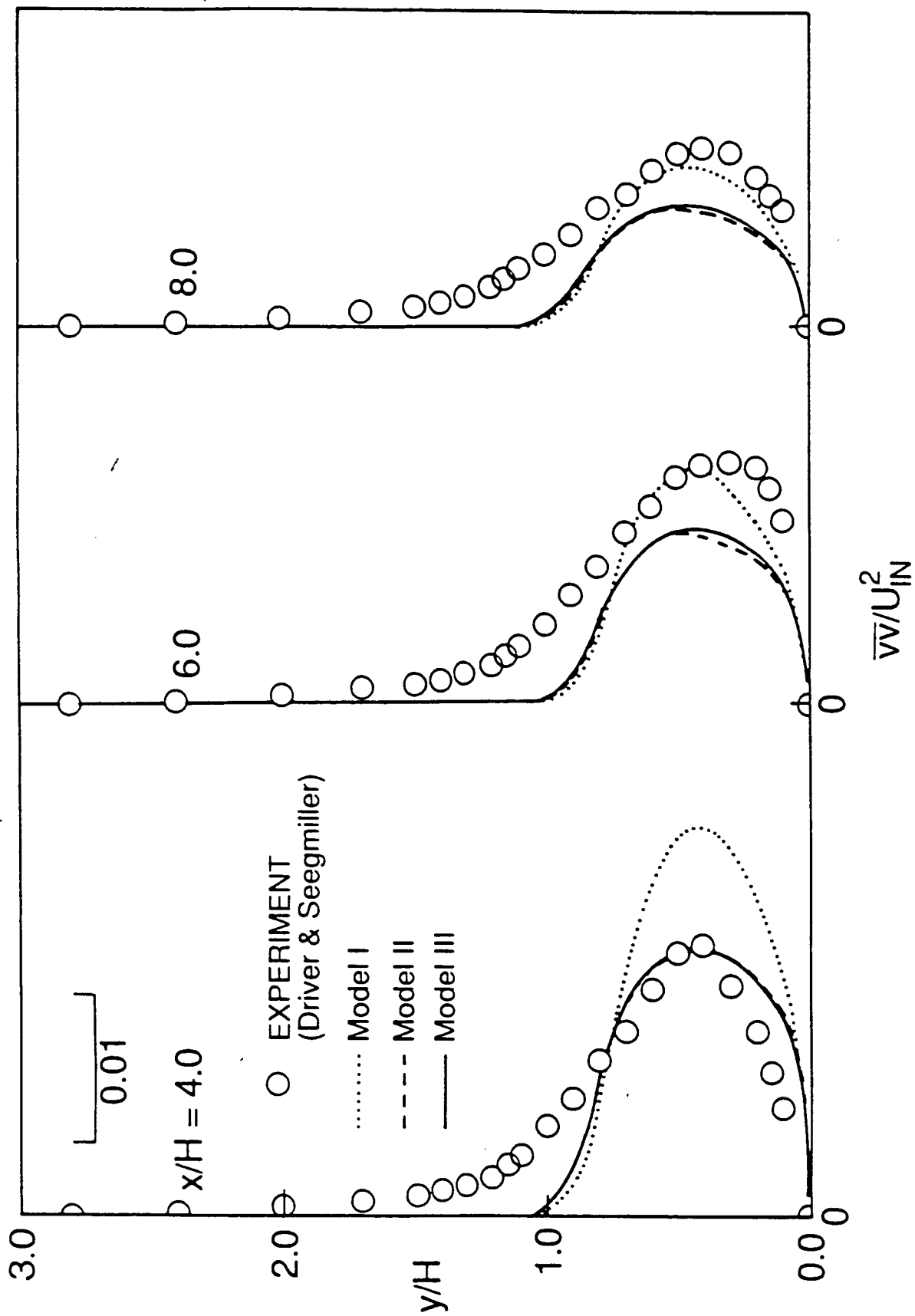


FIGURE 4.11 $\overline{v^2}$ -profiles behind the step. Comparison with data of Driver and Seegmiller

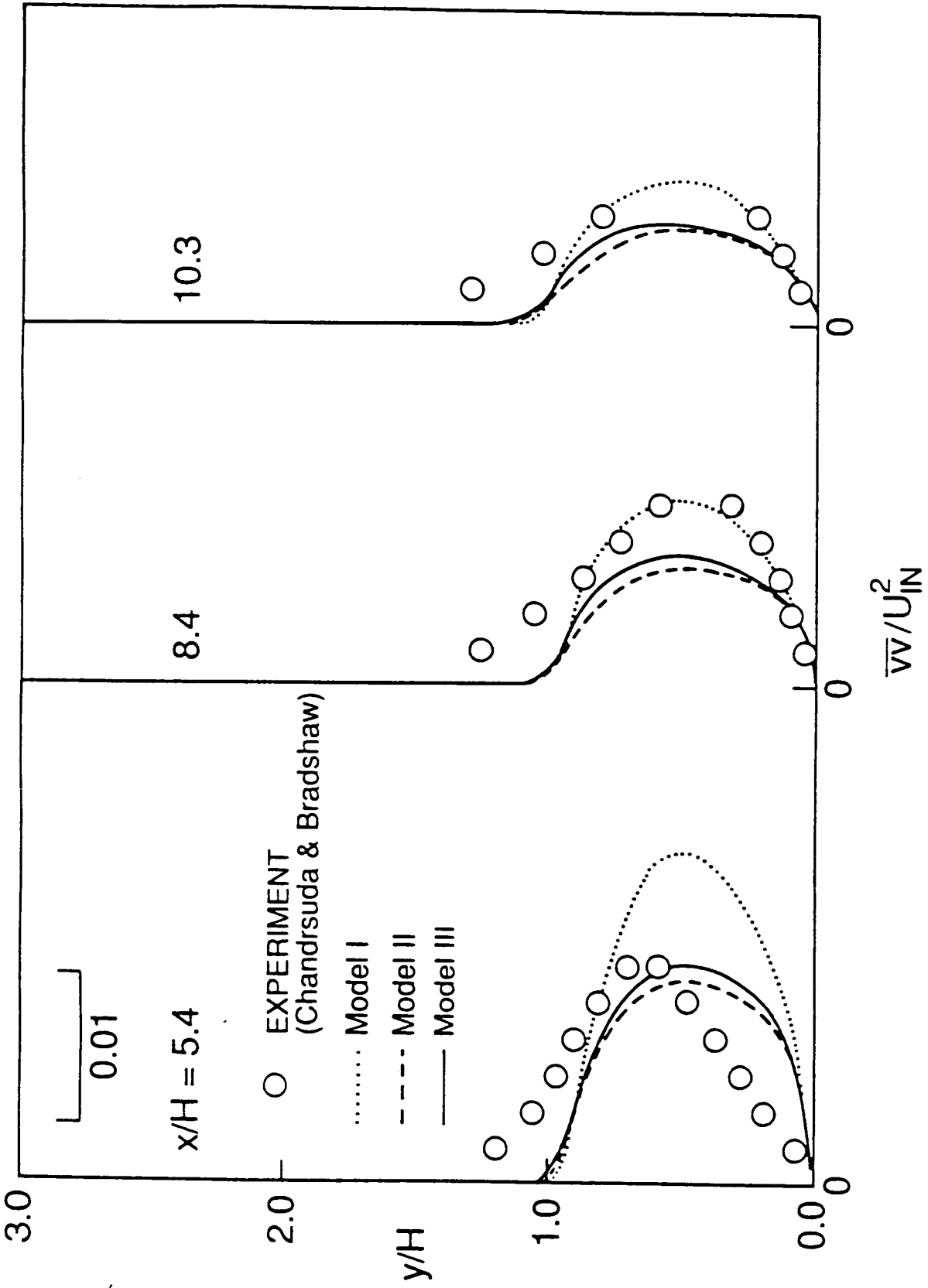


FIGURE 4.12 $\overline{v^2}$ profiles behind the step. Comparison with data of Chandrsuda and Bradshaw

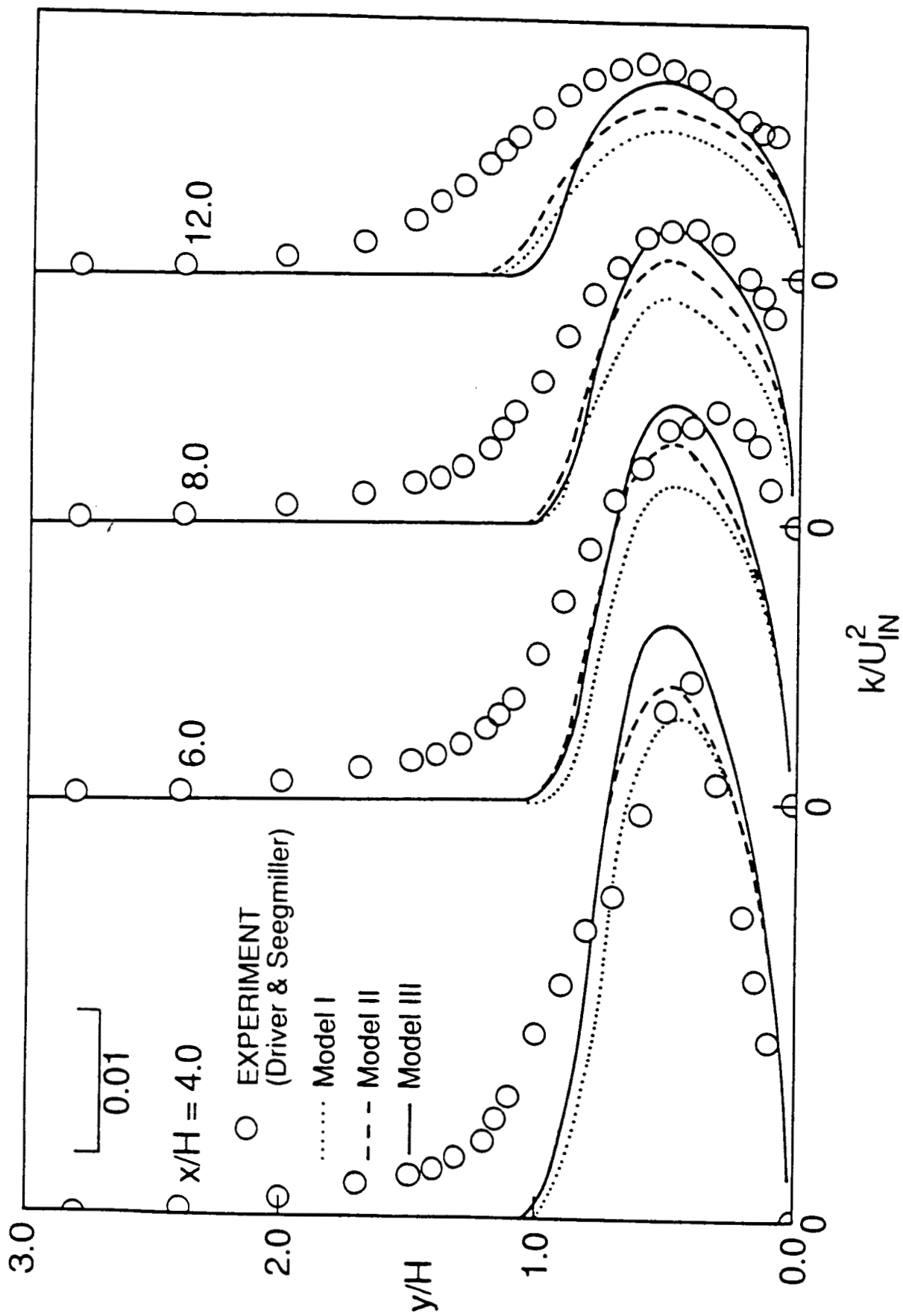


FIGURE 4.13 k -profiles behind the step. Comparison with data of Driver and Seegmiller

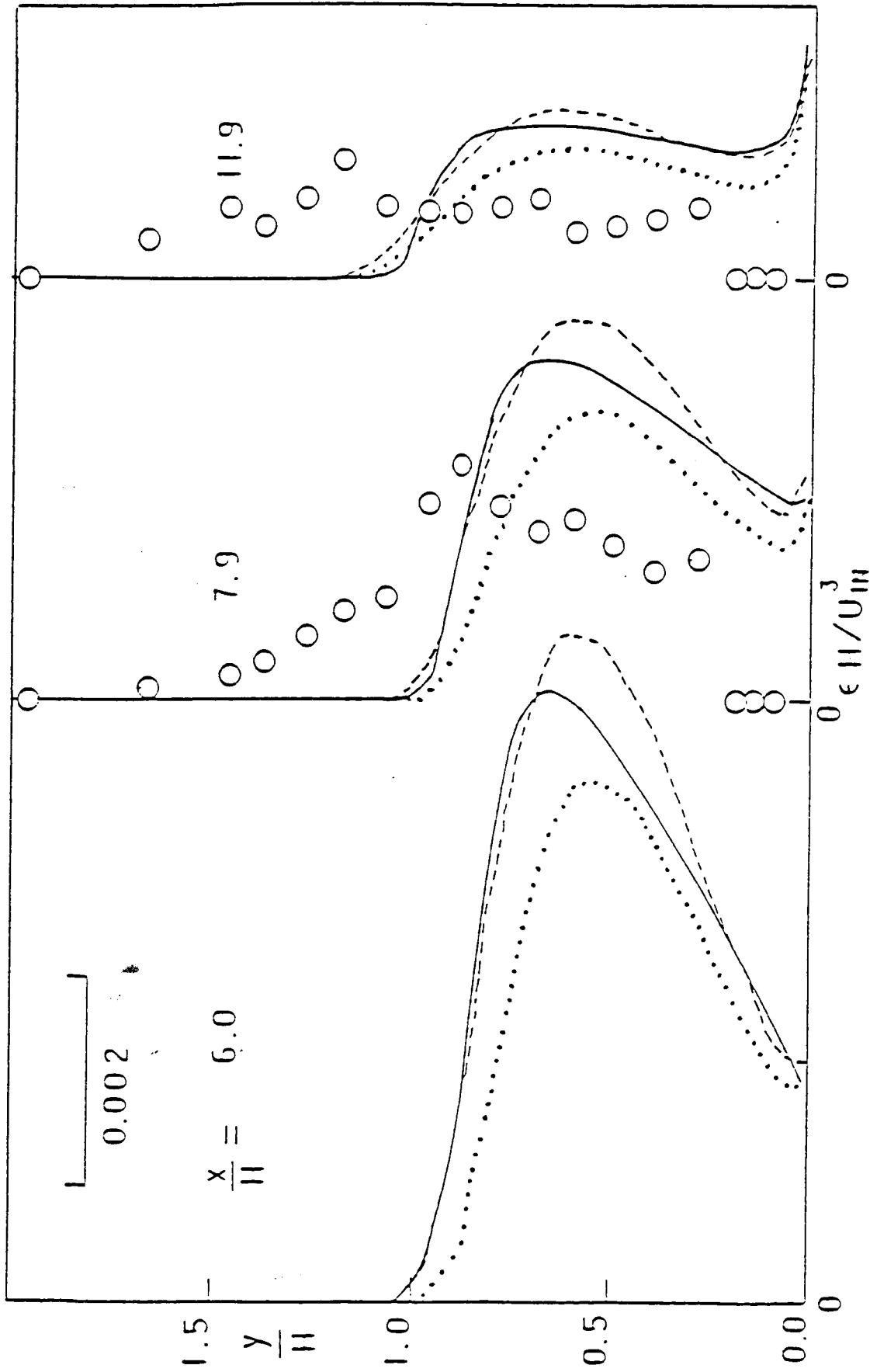


FIGURE 4.14 ϵ -profiles behind the step. Comparison with data of Driver and Seigmiller

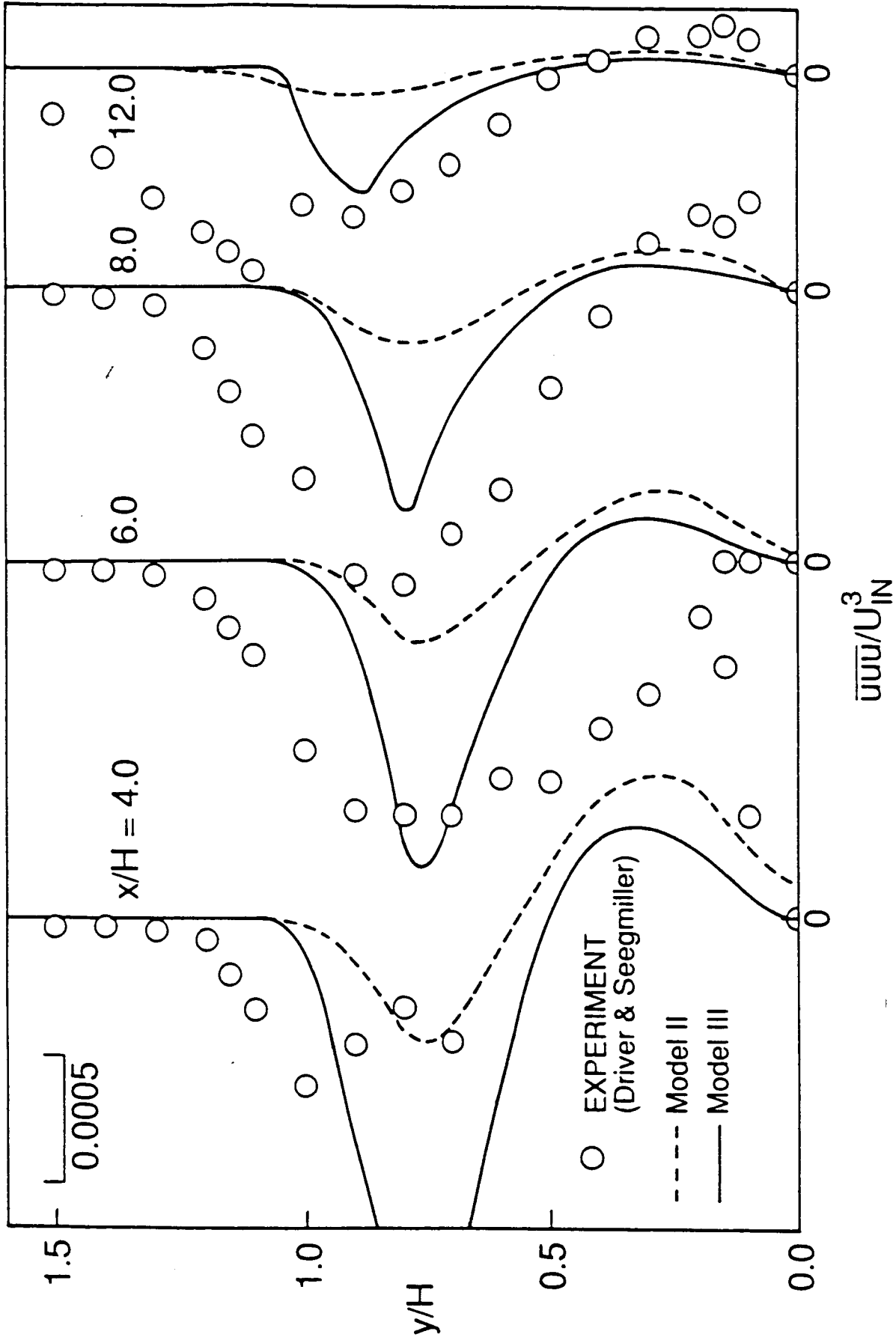


FIGURE 4.15 \overline{uuu} -profiles behind the step. Comparison with data of Driver and Seegmiller

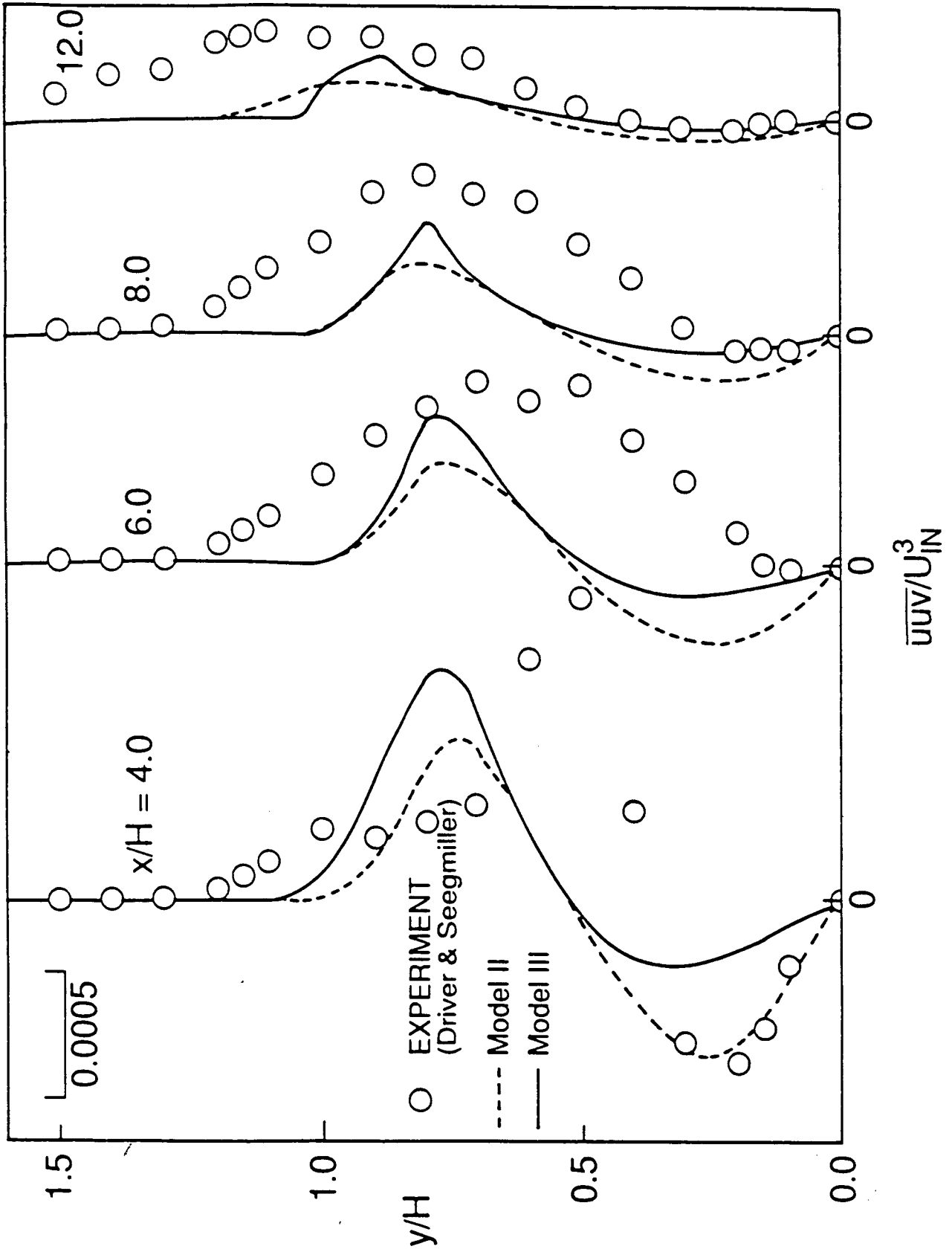


FIGURE 4.16 \overline{uuv} -profiles behind the step. Comparison with data of Driver and Seegmiller

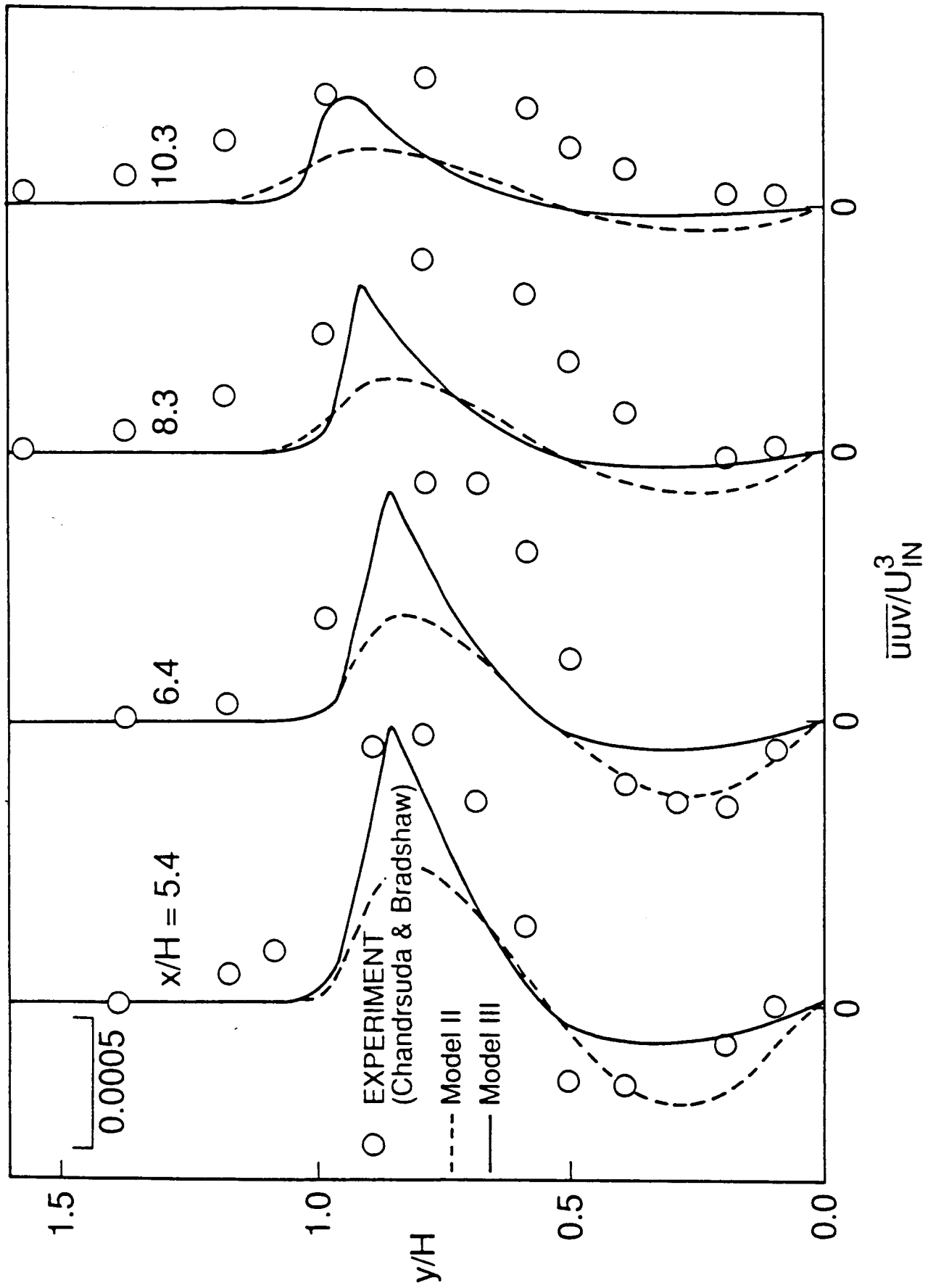


FIGURE 4.17 \overline{uuv} -profiles behind the step. Comparison with data of Chandrsuda and Bradshaw

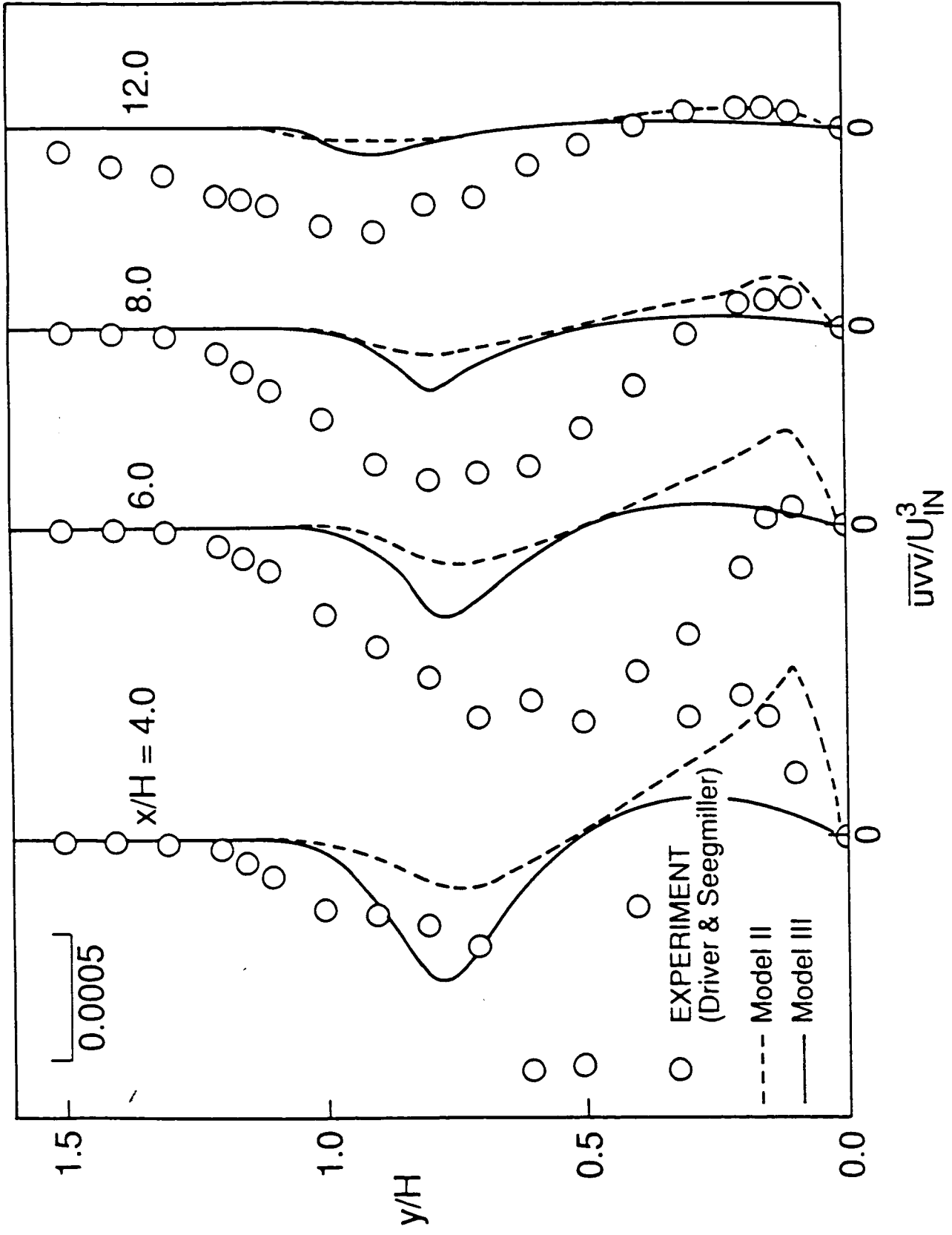


FIGURE 4.18 \overline{uvv} -profiles behind the step. Comparison with data of Driver and Seegmiller

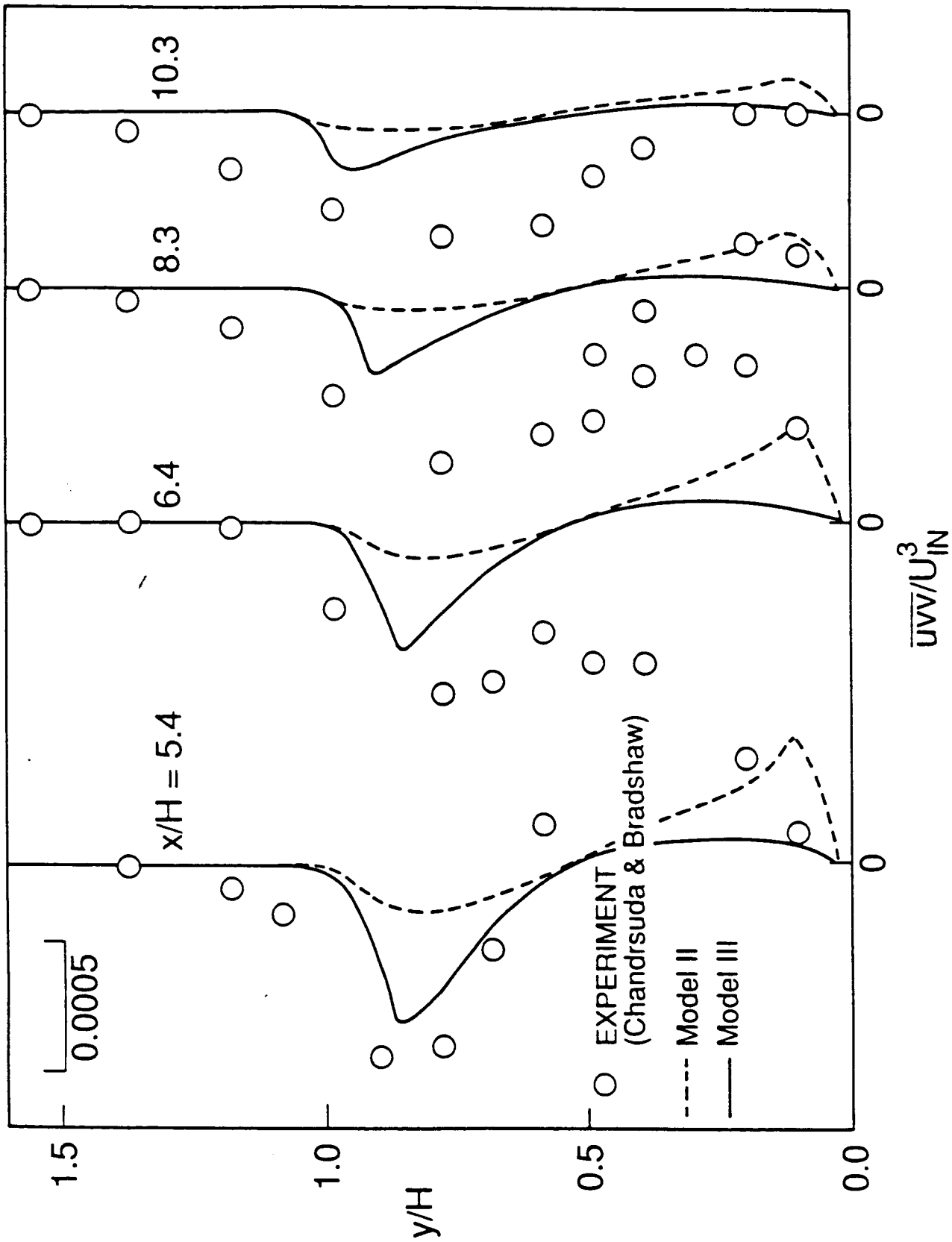


FIGURE 4.19 \overline{uvw} -profiles behind the step. Comparison with data of Chandrsuda and Bradshaw

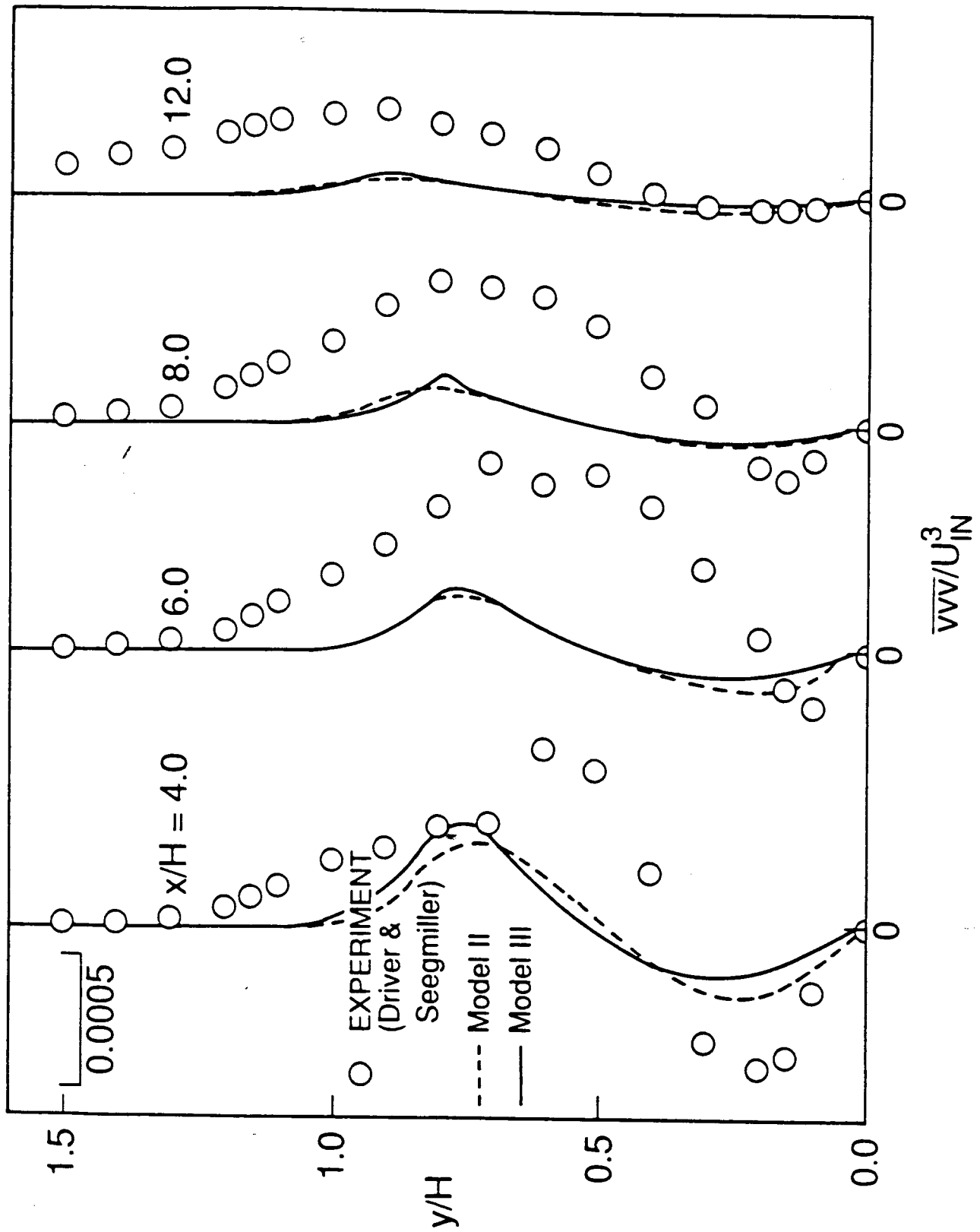


FIGURE 4.20 $\overline{v_w}$ -profiles behind the step. Comparison with data of Driver and Seegmiller

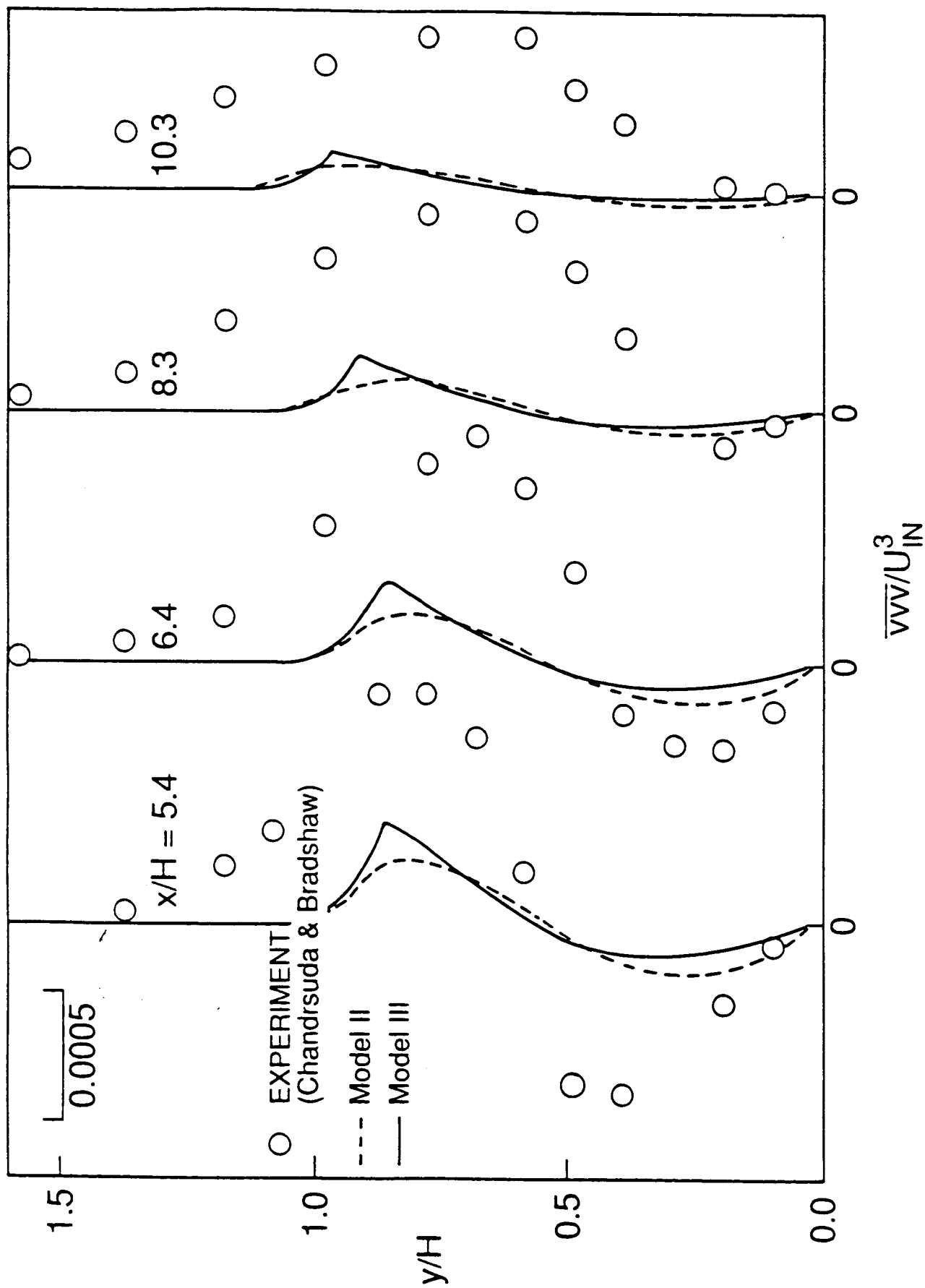


FIGURE 4.21 $\overline{v'v'}$ -profiles behind the step. Comparison with data of Chandrsuda and Bradshaw